Chapter 4

RESULTS & DISCUSSION

4.1 In-Silico studies

4.1.1 Molecular target 1: Bcl-2

4.1.1.1 Approach 1

Molecular docking results revealed that quercetin and taxifolin bound to hydrophobic groove of Bcl-2 with binding energy -28.56 and -30.66 Kj/Mol respectively (Fig 4.1). Quercetin showed hydrogen bonding with Arg129, Tyr108, Gln118 and His120 along with π-cation interaction with His120. Taxifolin showed similar interaction as quercetin and showed hydrogen bonding with Arg129, Tyr108, Gln118 and His120.

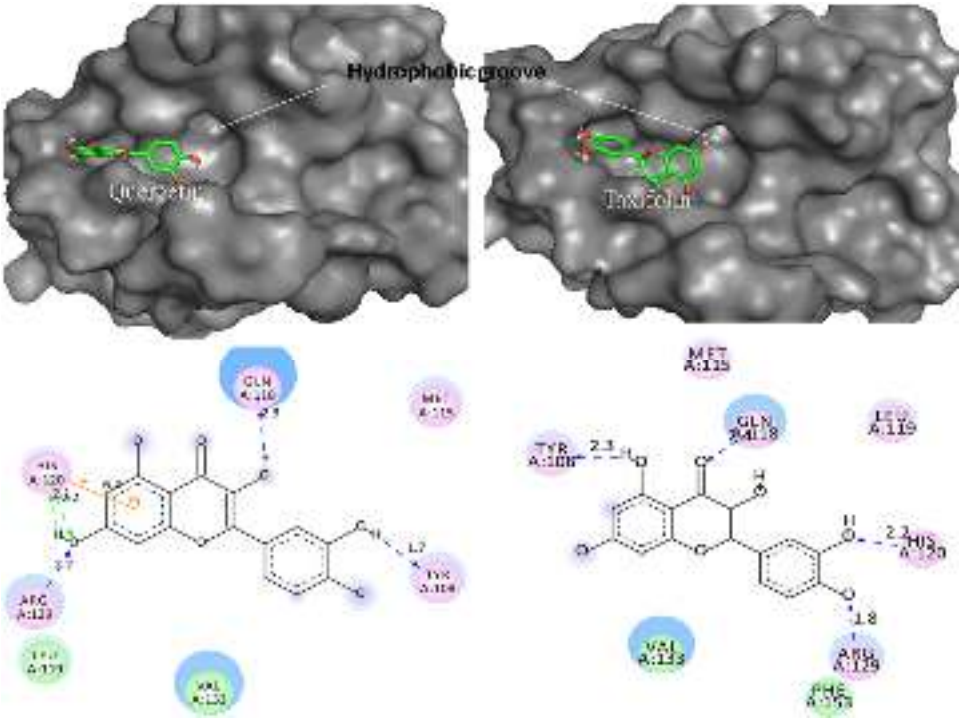

Fig 4.1 Ligand docked Bcl-2: Left; quercetin (upper-surface presentation of Bcl-2-quercetin complex, lower-2D plot of interaction of quercetin with Bcl-2), Right; taxifoin (upper- surface presentation of Bcl-2-taxifoin complex, lower-2D plot of

interaction of taxifolin with Bcl-2) (Published in Verma et al., Journal of Biomolecular Structure and Dynamics, 33, 5, 1094–1106, 2015.)

The lowest binding energy (most negative) docking conformation generated by Autodock was taken as initial conformation for MD simulation. The time dependent behavior of MD trajectories for Bcl-2-Bax-ligand complex including root mean square deviation (RMSD) for all backbone atoms, short range (SR) van der Waals and electrostatic energies along with essential dynamics was analyzed. Fig. 4.2A showed that the RMSD profiles were always less than 0.30 nm for both quercetin and taxifolin bound Bcl-2 backbone during the entire simulation suggesting the stability of Bcl-2 in ligand bound state and suitability for post analysis. Fig. 4.2B showed the RMSD profile of ligands bound to Bcl-2 pocket. Quercetin showed increase in RMSD after ~3 ns for very short time interval while taxifolin showed more stable profile as compared to quercetin throughout the simulation. These results showed the stable binding of ligands in the hydrophobic pocket of Bcl-2.

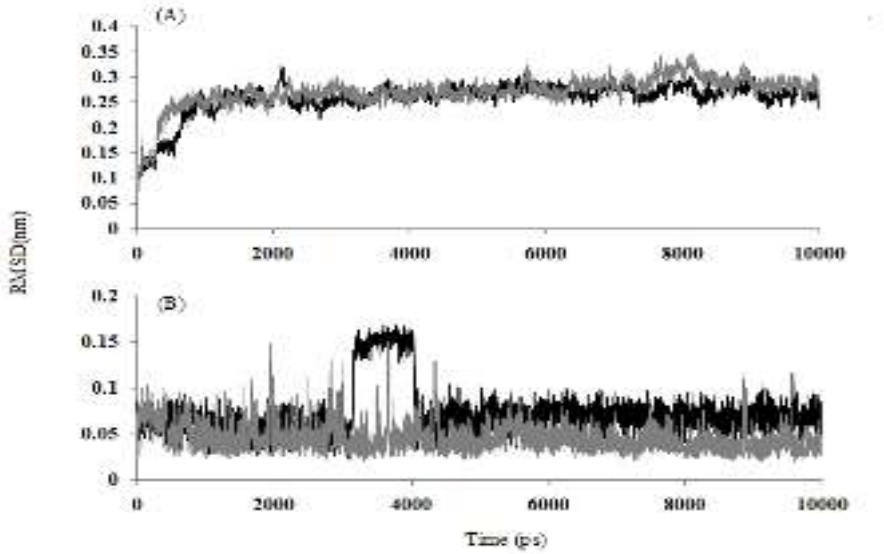

Fig 4.2 (A) Plot of root mean square deviation (RMSD) of backbone of Bcl-2 bound to quercetin (black) and taxifolin complex (grey), (B) Plot of root mean square deviation (RMSD) of quercetin (black) and taxifolin (grey) in hydrophobic groove of Bcl-2 (Published in Verma et al., Journal of Biomolecular Structure and Dynamics, 33, 5, 1094–1106, 2015.)

.

To explore the interaction between the ligands and the Bcl-2, the energy contributions of short range (SR) van der Waals and electrostatic interaction energies were calculated. Quercetin interaction with Bcl-2 was dominated by short range (SR) van der Waals energies with average value –151.13 kJ/mol while the average value of SR electrostatic energies was –8.90 kJ/mol. Similar to quercetin, the van der Waals energy between taxifolin and Bcl-2 during the simulation was approximately –18.23 kJ/mol on average. However, the average short-range (SR) electrostatic energy was approximately –161.31 kJ/mol (Fig 4.3A, B). It was observed that short range (SR) van der Waals energy play main role in the interaction with Bcl-2 and ligand binding.

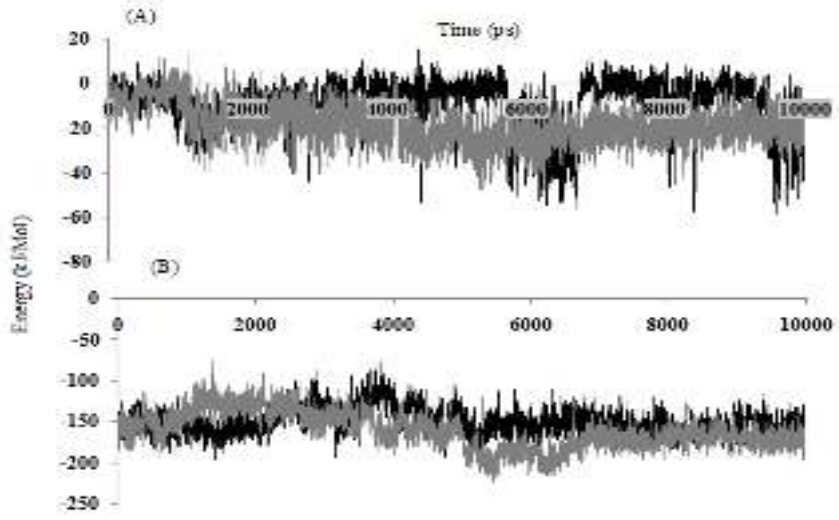

Fig 4.3 Profile of (A) Coulombic interaction energy, (B) van der Waals (vdW) interaction energy between Bcl-2-quercetin (black) and Bcl-2-taxifolin (grey) (Published in Verma et al., Journal of Biomolecular Structure and Dynamics, 33, 5, 1094–1106, 2015.)

.

To elucidate the residues of hydrophobic groove of Bcl-2 which were involved in a stable interaction with ligands, 2D plots of interaction were generated using Discovery studio 3.1. Quercetin showed strong π–π and π–sigma interaction with Tyr108 and π–π with His120 along with h-bonding with Met115, Gln118 and Arg 139 (Fig 4.4).

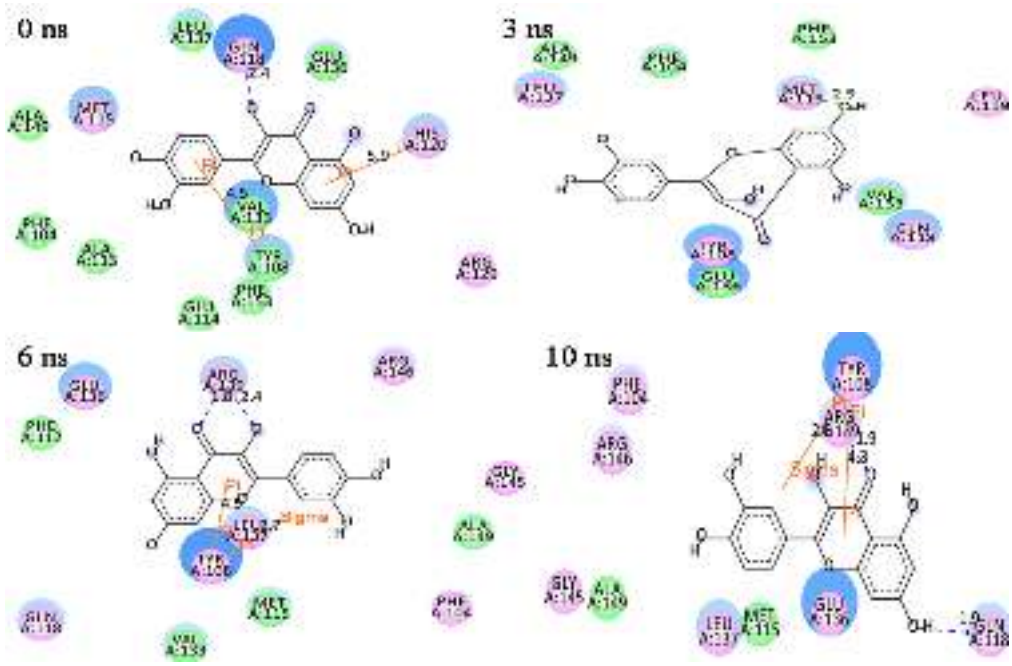

Fig. 4.4 2D presentation of interaction of quercetin with Bcl-2 residues at different time of MD simulation (Published in Verma et al., Journal of Biomolecular Structure and Dynamics, 33, 5, 1094–1106, 2015.)

.

Taxifolin showed strong π–sigma interaction with Val133 and π–cation with Arg129 along with h-bonding with His120 and Thr 122 (Fig 4.5).

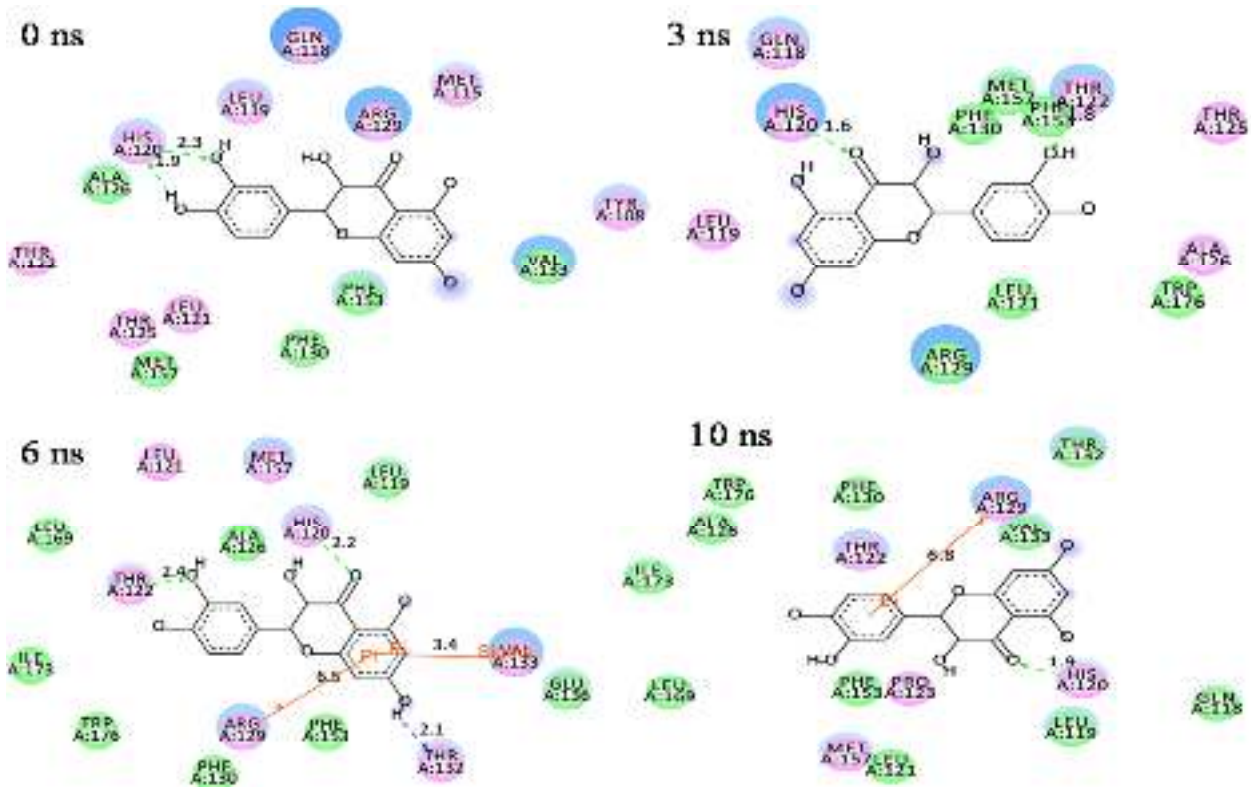

Fig. 4.5 2D presentation of interaction of taxifolin with Bcl-2 residues at different time of MD simulation (Published in Verma et al., Journal of Biomolecular Structure and Dynamics, 33, 5, 1094–1106, 2015.)

.

Comparative analysis of final pose of Bcl-2-ligand complex after 10 ns molecular dynamics simulation with crystal structure of Bcl-2 revealed that binding of the quercetin and taxifolin bring significant conformational changes in the Bcl-2 structure. Fig. 4.6 clearly indicates the collapse of hydrophobic groove in the ligand bound Bcl-2. However taxifolin showed higher effect on the groove and found to be completely disappear in taxifolin bound Bcl-2. All these results indicated that polyphenols have potential to inhibit the Bcl-2 by binding with apoptotic protein and

distorting structure of hydrophobic groove.

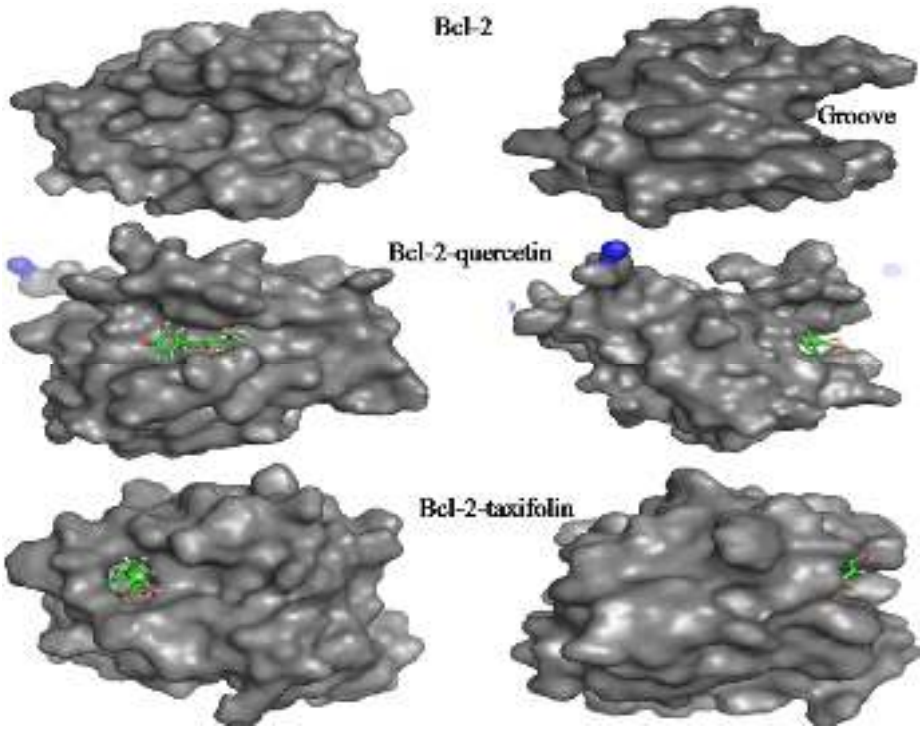

Fig. 4.6 comparison of surface structure of Bcl-2 crystal structure and ligand bound Bcl-2 after 10 ns MD simulation (Published in Verma et al., Journal of Biomolecular Structure and Dynamics, 33, 5, 1094–1106, 2015.)

.

It is clear that antiapoptotic Bcl-2 proteins effectively inhibit apoptosis, at least in part by directly binding to proapoptotic Bcl-2 proteins such as Bim, Bax, Bid, and Bad. Experimentally determined three-dimensional structures of Bcl-2 showed that these proteins contain a well-defined hydrophobic surface binding groove, known as the BH3 binding groove, into which Bid, Bax, Bim, Bad, or Noxa binds. 9–11 Small molecules designed to bind to the BH3 binding groove of these antiapoptotic Bcl-2 proteins and to block their interactions with proapoptotic Bcl-2 members were predicted to promote apoptosis in cancer cells and represented a promising new cancer therapeutic strategy. There are several modeling studies which

showed the binding of inhibitors to hydrophobic groove (Petros et al., 2001; Sattler et al., 1997; Petros et al., 2000; Tang et al., 2008; Zhou et al., 2012) but the collapse of hydrophobic groove on ligand binding was reported first time. These results may lead to the conclusion that quercetin and taxifolin efficiently bind to hydrophobic groove and alter the structure by inducing conformational changes. Taxifolin was found more efficient as compared to quercetin in terms of interaction energy and collapse of hydrophobic groove.

4.1.1.2 Approach 2

Molecular docking results revealed that quercetin, taxifolin and obatoclax bound to Bcl-2-Bax complex. The interacting residues were Arg 65, Asp 68, Glu 69, and Ser 72 of Bax and Arg 110, and Asp 111 of Bcl-2 as shown in Fig 4.7

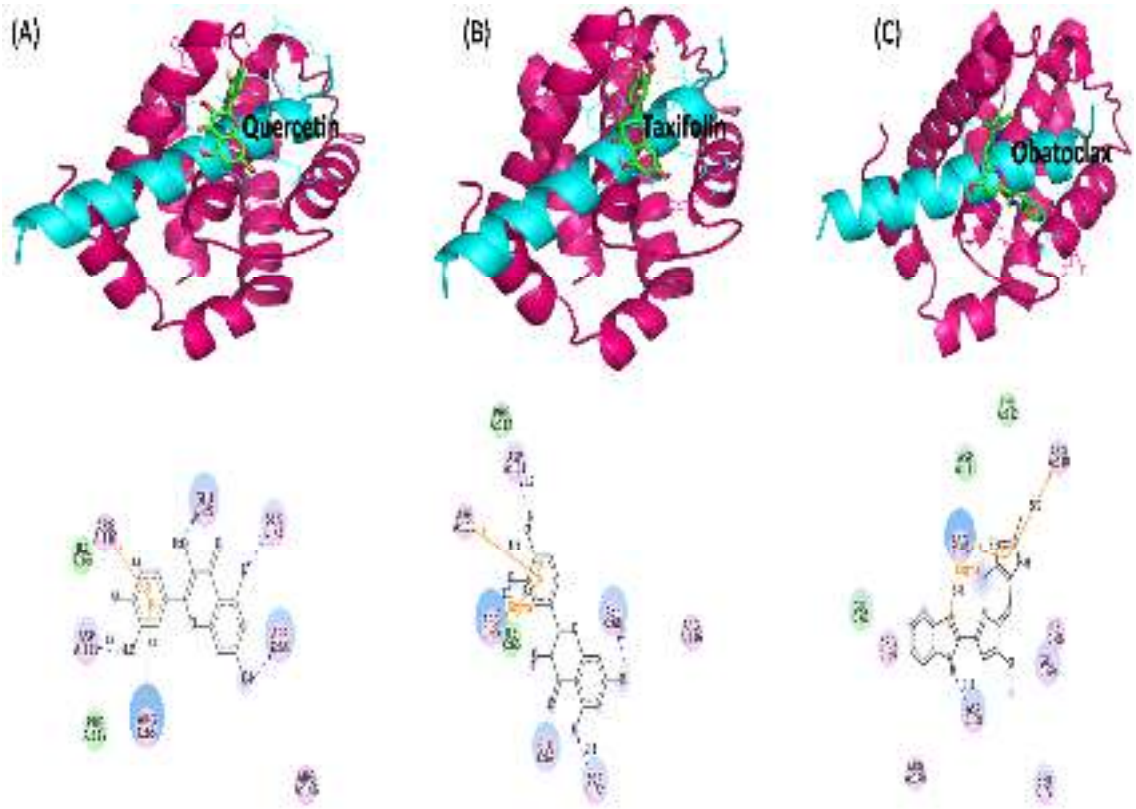

Fig 4.7 Ligand docked Bcl-2-Bax complex (A) quercetin (upper-cartoon presentation of Bcl-2-Bax-quercetin complex, lower-2D plot of interaction of quercetin with Bcl-2-Bax complex), (B) taxifoin (upper-cartoon presentation of Bcl-2-Bax-taxifoin complex, lower-2D plot of interaction of taxifolin with Bcl-2-Bax complex), (C) obatoclax (upper-cartoon presentation of Bcl-2-Bax- obatoclax complex, lower-2D plot of interaction of obatoclax with Bcl-2-Bax complex) (Published in Verma et al., Journal of Biomolecular Structure and Dynamics, 33, 5, 1094–1106, 2015.)
.

Previous studies showed that Asp 68 of Bax play crucial role in the interaction with Bcl-2. Mutation analysis of this residue to alanine revealed remarkable decrease in the interaction with Bcl-2. However, Lys 64, Arg 65 Glu 69 and Asp 71 are also important for this interaction but the Asp 68 regarded as key for Bcl-2-Bax interaction (Pintoa et al., 2004; Ku et al., 2011). As the interaction of Bcl-2 and Bax is depend on a number of residues, on the basis of previous studies, we had selected those ligand docked complexes, to carry out molecular dynamic simulation, were selected in which ligands were found to interact with key residues Asp 68. Fig. 4.8A showed that the RMSD profiles were always less than 0.25 nm for ligand unbound Bcl-2-Bax complex during the entire simulation suggesting the stability of Bcl-2-Bax complex in ligand unbound state. An initial steep rise in the RMSD for the first, ~1000 ps and subsequently a constant profile was observed for the Bcl-2-Bax complex. RMSD profile along with snapshots recorded at different time intervals (Fig 4.8B) of MD simulation revealed the stability of ligand unbound Bcl-2-Bax complex.

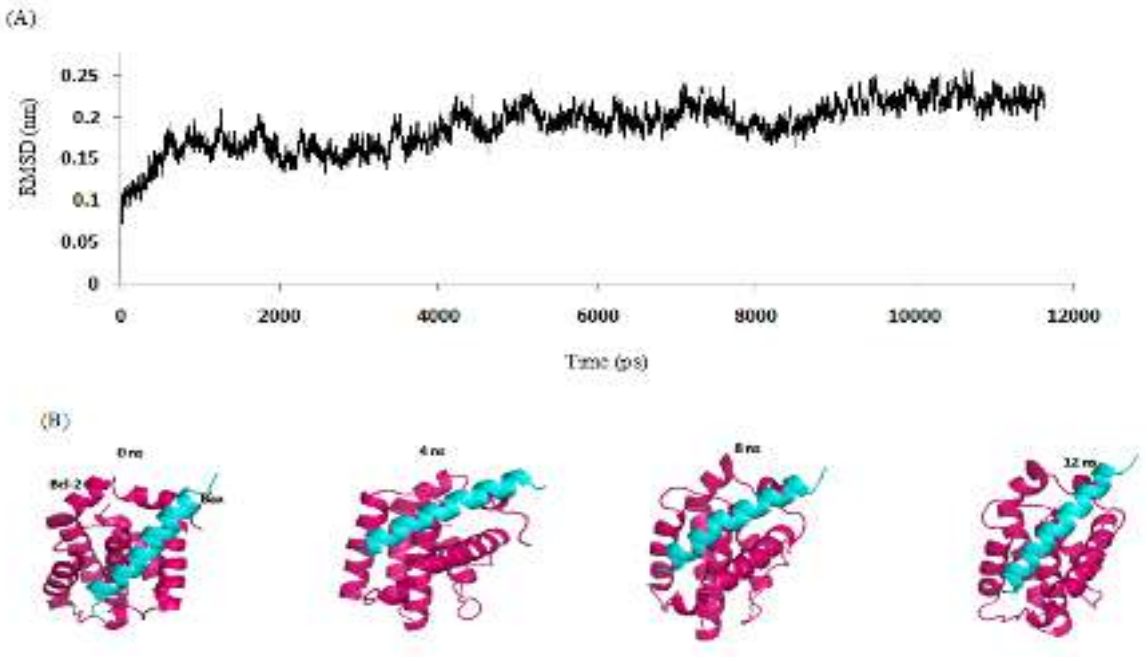

Fig 4.8. (A) RMSD profile of Bcl-2-Bax backbone, (B) conformations of Bcl-2-Bax complex during 12 ns MD simulation (Published in Verma et al., Journal of Biomolecular Structure and Dynamics, 33, 5, 1094–1106, 2015.)

.

Fig. 4.9A shows that the RMSD profile of taxifolin bound Bcl-2-Bax was always less than 0.25 nm up to ~7000 ps afterward a high rise in the RMSD was observed subsequently a constant profile was observed with up and down for very small time intervals. This increase in RMSD was found to be in the good agreement with the snapshots recorded after 7000 ps which revealed the separation of Bax peptide from Bcl-2 (Fig 4.9B).

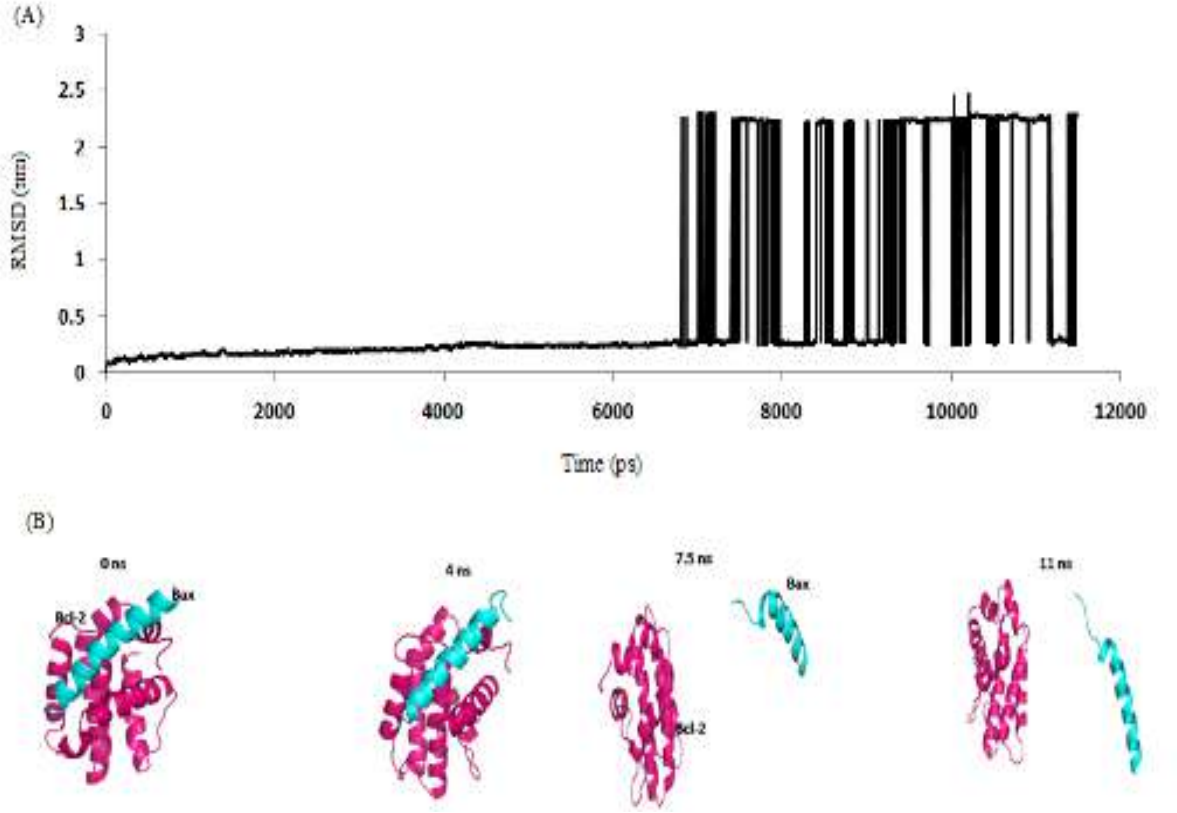

Fig 4.9. (A) RMSD profile of taxifolin bound Bcl-2-Bax complex backbone, (B) conformations of taxifolin bound Bcl-2-Bax complex during 12 ns MD simulation showed dissociation of complex (Published in Verma et al., Journal of Biomolecular Structure and Dynamics, 33, 5, 1094–1106, 2015.)

.

In quercetin bound Bcl-2-Bax complex, the RMSD profile of backbone showed high increase from the value of 0.25 nm after ~5000 ps and subsequently a more or less constant profile was observed followed by high increase in RMSD (Fig. 4.10A). Similar to taxifolin, this increase of RMSD was found to be associated with the dissociation of Bcl-2-Bax complex as evidenced by recorded snapshots (Fig. 4.10B).

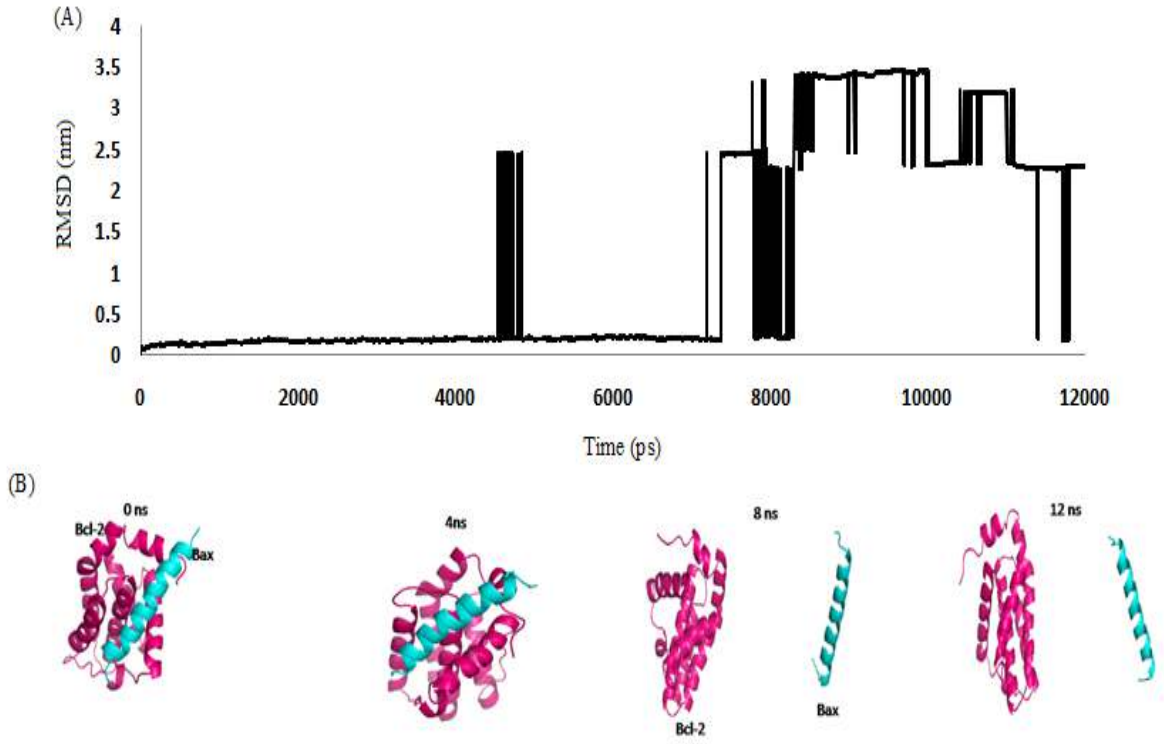

Fig 4.10. (A) RMSD profile of quercetin bound Bcl-2-Bax complex backbone, (B) conformations of quercetin bound Bcl-2-Bax complex during 12 ns MD simulation showed dissociation of complex (Published in Verma et al., Journal of Biomolecular Structure and Dynamics, 33, 5, 1094–1106, 2015.)

.

However in case of obatoclax complexed Bcl-2-Bax showed constant profile at 0.25 nm with increase at ~8000 ps for very short time interval (Fig. 4.11A). Snapshots, further, confirmed that obatoclax not showed significant disruption effect on Bcl-2-Bax (Fig 4.11B) which favored the previous experimental results (Samuel et al., 2010).

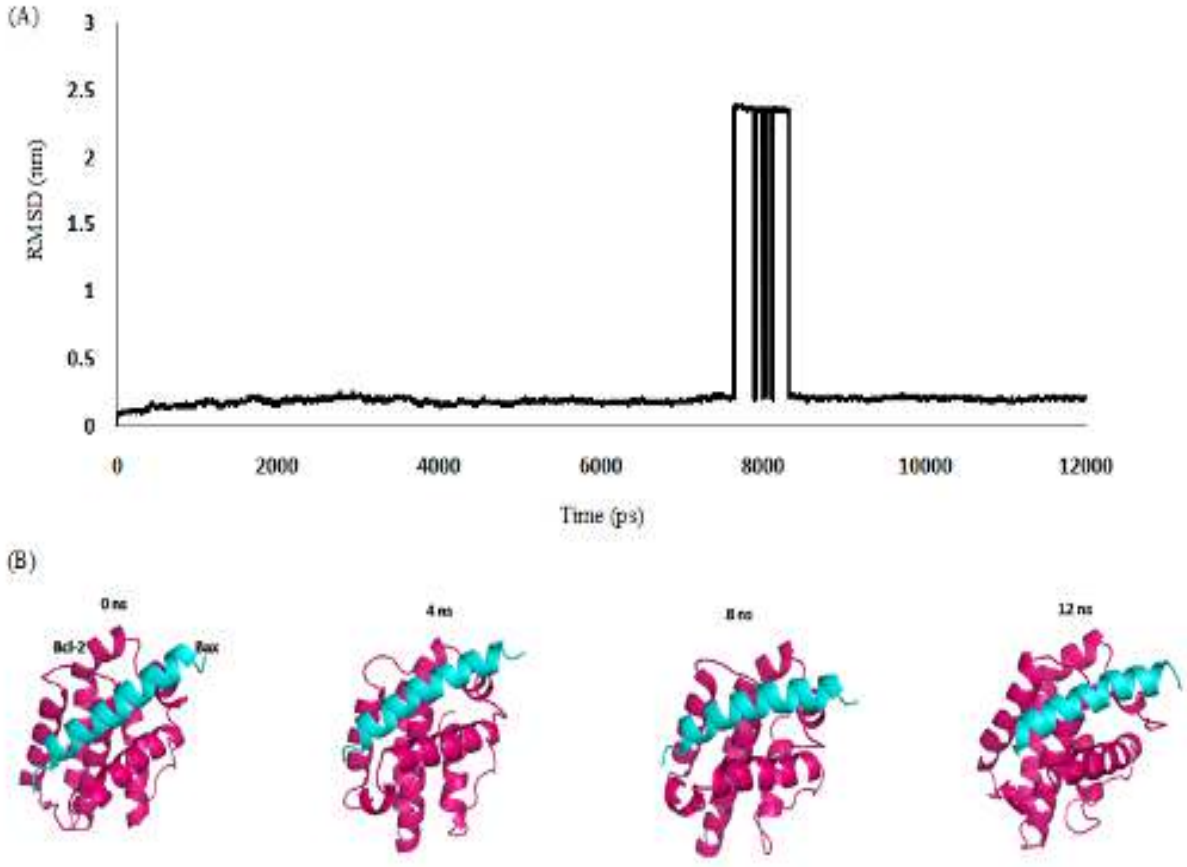

Fig 4.11 (A) RMSD profile of obatoclax bound Bcl-2-Bax complex backbone, (B) conformations of obatoclax bound Bcl-2-Bax complex during 12 ns MD simulation showed insignificant dissociation effect (Published in Verma et al., Journal of Biomolecular Structure and Dynamics, 33, 5, 1094–1106, 2015.)

.

These results suggest that taxifolin and quercetin disrupted the Bcl-2-Bax stable interaction during 12 ns MD simulation while obatoclax not did so as reported by previous studies.

To identify the flexible regions of the proteins, RMSF of backbone from its time averaged position was analyzed. The RMSF profile of protein backbone revealed higher fluctuation in taxifolin and quercetin bound complex as compared to ligand unbound and obatoclax bound form during the course of simulation. This

suggests that binding of taxifolin and quercetin made backbone more flexible to move. Further, the flexibility of Bax peptide backbone was found more as compared to Bcl-2. This might be due to the restriction caused by interaction of taxifolin and quercetin to Bcl-2 (Fig 4.12).

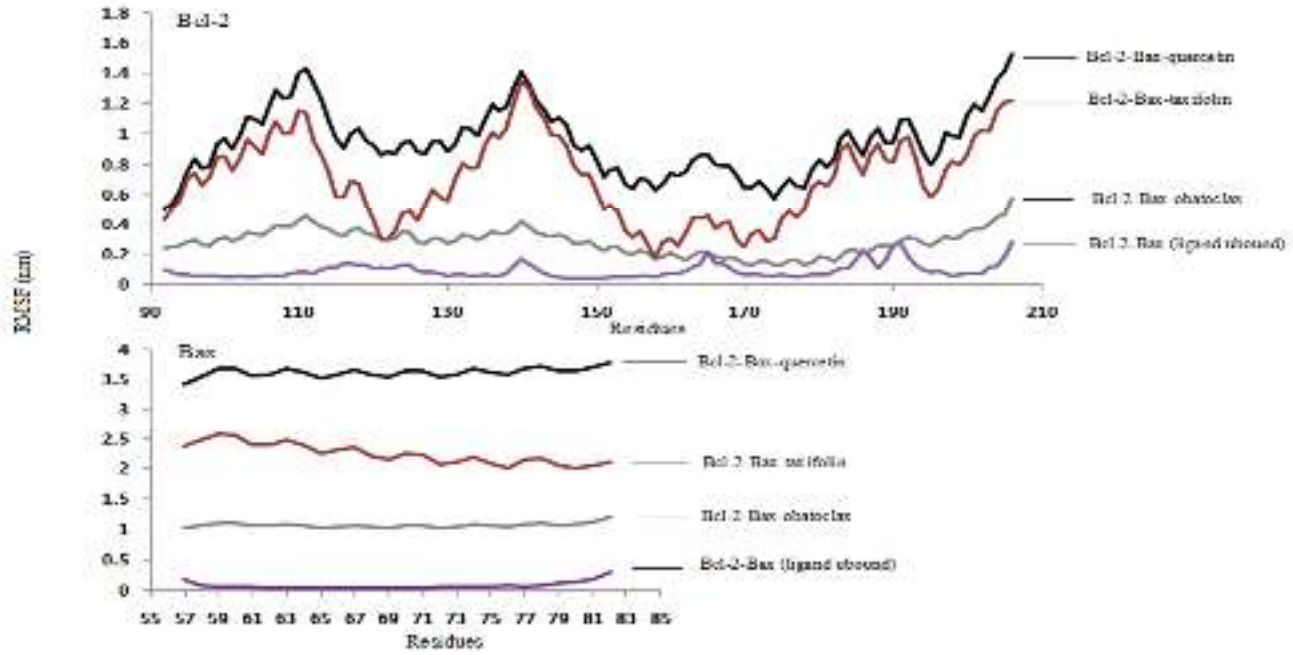

Fig 4.12. RMSF of Bcl-2 residues backbone (upper) and Bax residues backbone (lower) during MD simulation (Published in Verma et al., Journal of Biomolecular Structure and Dynamics, 33, 5, 1094–1106, 2015.)

.

The RMSF profile of interface residue side chains also suggested higher fluctuation in taxifolin and quercetin bound complex as compared to unbound and obatoclax bound (Fig 4.13).

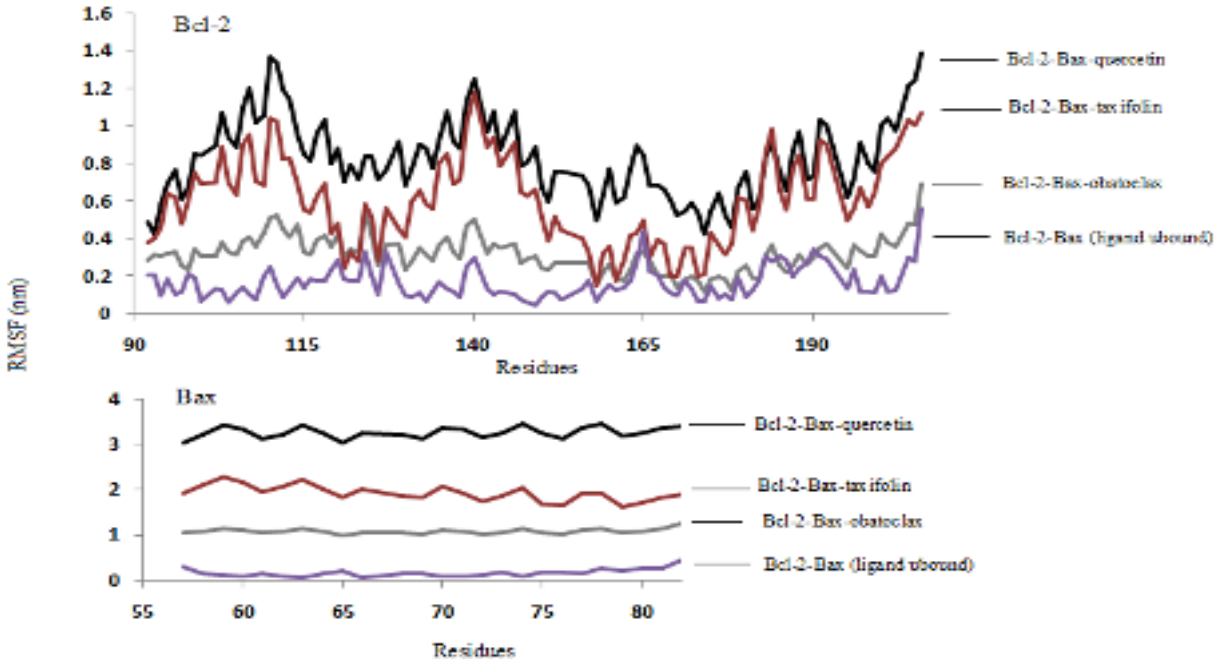

Fig 4.13. RMSF of Bcl-2 residues side chain (upper) and Bax residues side chain (lower) during MD simulation (Published in Verma et al., Journal of Biomolecular Structure and Dynamics, 33, 5, 1094–1106, 2015.)

.

These results suggested that binding of taxifolin and quercetin disrupted the stable interactions of these residues at the Bcl-2-Bax interface which remained consistent in ligand unbound form. The authenticity of MD simulations performed in the study favored by the experimental results for insignificant disruption effect of obatoclax on Bcl-2-Bax complex.

4.1.2 Molecular target 2: Heat shock protein 90

4.1.2.1 Approach 1: Interaction of taxifolin with Hsp90

Docking studies revealed that taxifolin was found to bind at ATP-binding site of Hsp90 with lowest binding energy of -31.08 KJ/Mol. Free energy of binding was calculated as a sum of four energy terms of intermolecular energy (van der Waals,

hydrogen bond, desolvation and electrostatic energy), total internal energy, torsional free energy and unbound system energy. The major interactions shown in the Hsp90-ATP-binding site were important H-bonds with Asn 51, Ser 52, Lys 58, Asp 93 and Gly 97 (Fig. 4.14).

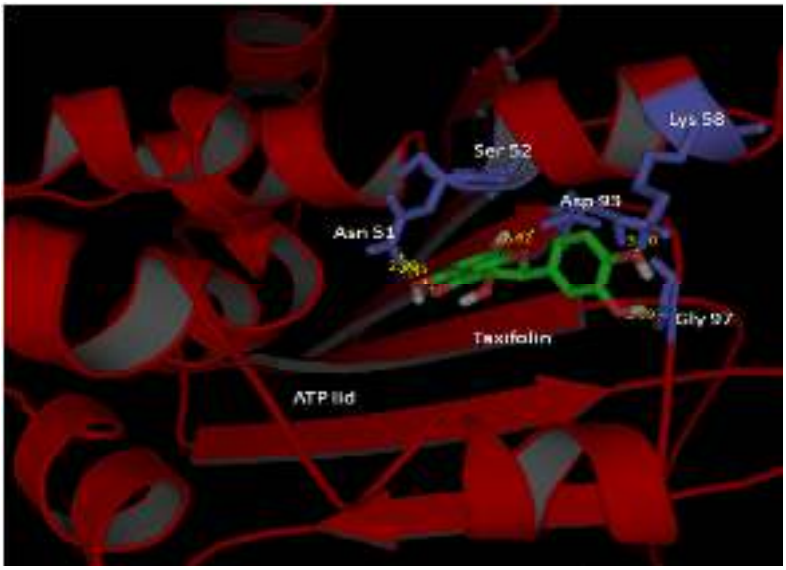

Fig 4.14. The Hsp90-ATP-binding site and taxifolin interaction.

The groups involved in H-bonding were hydroxyl (hydrogen donor), and carbonyl (hydrogen acceptor) group of taxifolin and NH (hydrogen donor) and oxygen atoms (hydrogen acceptor) of side chain or backbone of residues.

The Hsp90-taxifolin complex with the binding energy of -31.08 KJ/Mol obtained using Autodock was used for carrying out MD simulation. The time dependent behavior of MD trajectories for Hsp90-taxifolin complex was analyzed. RMSD of backbone atoms with respect to the initial conformation was calculated as a function of time to assess the conformational stability of the protein during the simulations. Fig. 4.15A showed that the RMSD profiles were always less than 0.3 nm

for the entire simulation which suggested the stability of Hsp90-taxifolin complex. An initial steep rise in the RMSD for the first, ~1000 ps and subsequently a constant profile was observed for the taxifolin bound Hsp90. Taxifolin unbound form showed slight higher RMSD after ~ 3500 ps. These results showed that the trajectories of the MD simulations after equilibrium were reliable for post analyses.

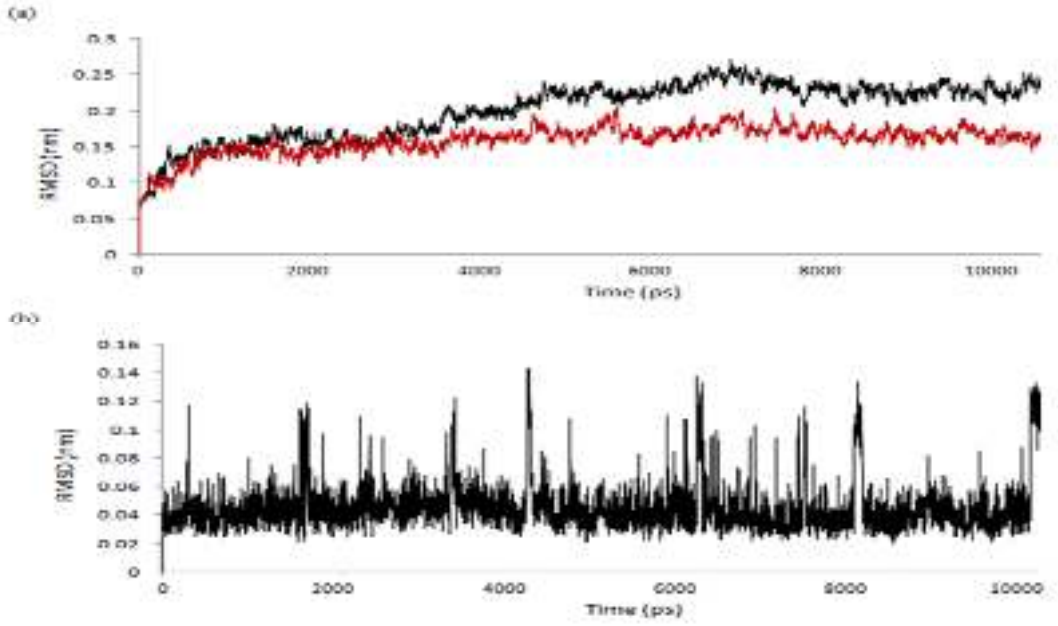

Fig. 4.15. (A) Plot of root mean square deviation (RMSD) of backbone of Hsp90 unbound (black) and Hsp90–taxifolin complex (red), (B) Plot of root mean square deviation (RMSD) of taxifolin. The trajectories were captured every 0.5 ps until the simulation time reached 10,000 ps **(**Published in Verma et al., Journal of Molecular Graphics and Modelling, 37, 27–38, 2012).

RMSD profile of taxifolin showed more or less constant pattern below 0.16 nm with marked fluctuation at different time interval (Fig. 4.15B). Analysis of taxifolin RMSD indicated that taxifolin showed remarkable stability for ATP-binding pocket during MD simulation. To investigate the thermodynamic stability of complex during

simulation, potential energy fluctuation was analyzed. The potential energy trajectories were adhered to constant values for the Hsp90-taxifolin complex during the entire simulation length. Number of H-bonds (cut off 0.35 nm) which were formed during MD simulation between taxifolin and Hsp90 also calculated. A variable profile was observed which fluctuate between 0 to 5 with an average value of 1.12 (Fig 4.16).

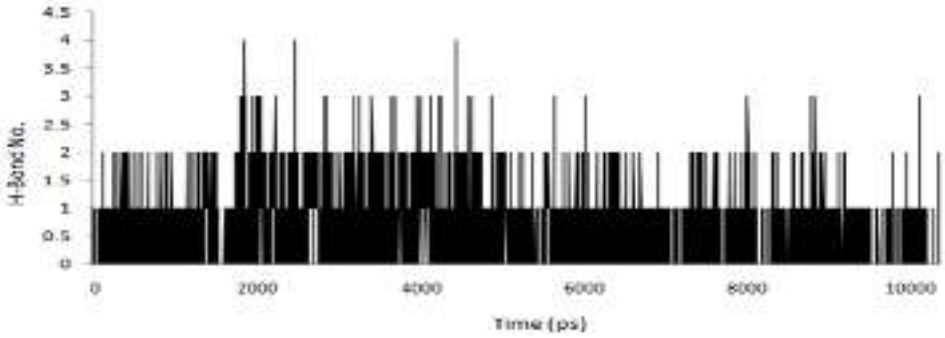

Fig. 4.16. Number of H-bonds formed between taxifolin and Hsp90 during 10,000 ps MD simulation **(**Published in Verma et al., Journal of Molecular Graphics and Modelling, 37, 27–38, 2012).

Apart from the H-bonds, hydrophobic interactions between taxifolin and binding site residues were also analyzed. 2D plots at the different time of simulation, generated by Discovery studio 3.1 (Accelrys Software Inc., 2011). Fig 4.17 revealed that side chain of residue Phe 138 involved in strong π-π interaction with aromatic ring of taxifolin. Taxifolin RMSD along with H-bonding and hydrophobic interaction analyses confirmed the stable interaction of taxifolin at ATP binding site of Hsp90.

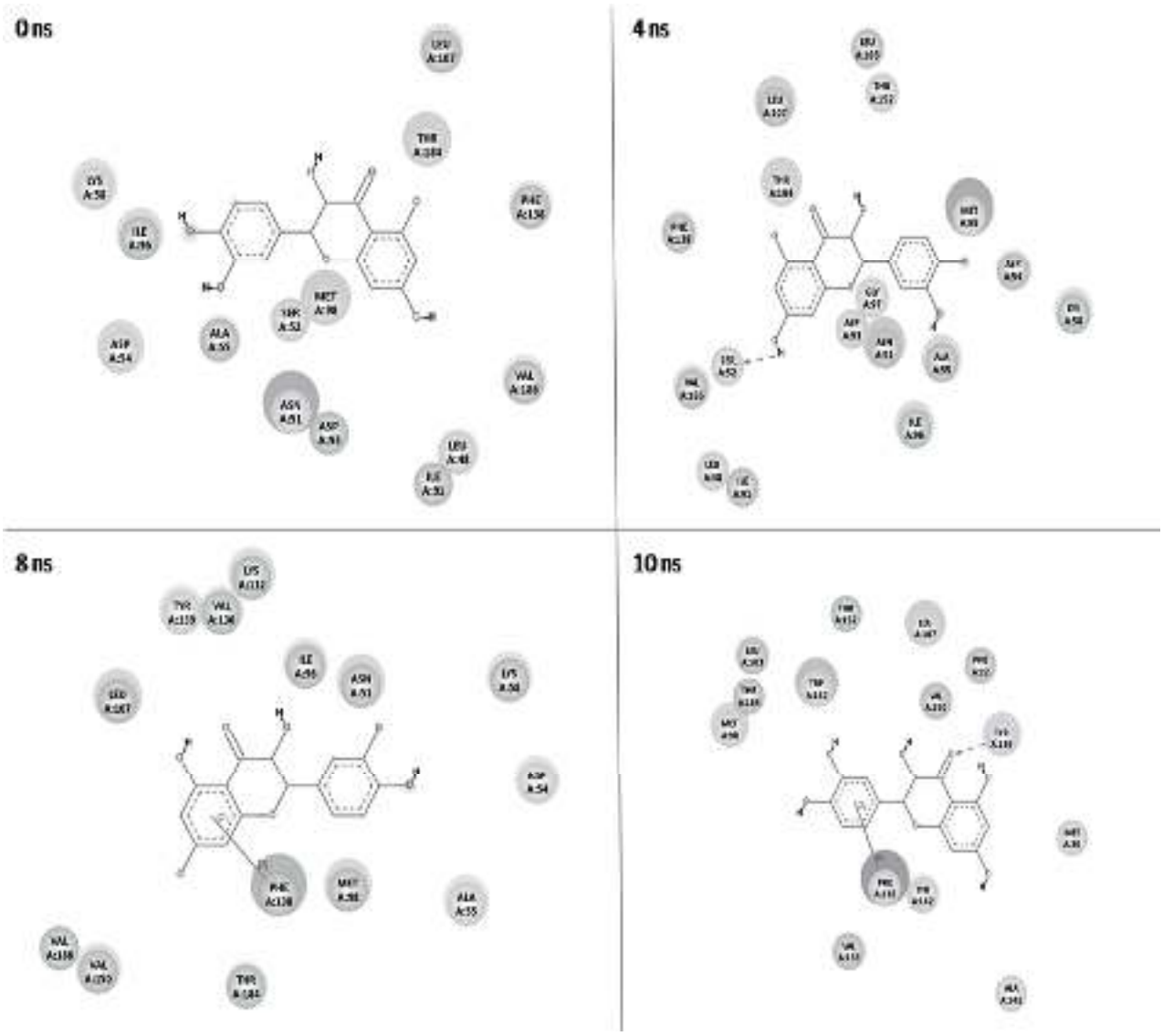

Fig. 4.17. 2D plots of interaction between taxifolin and Hsp90 at different time interval of MD simulation (Published in Verma et al., Journal of Molecular Graphics and Modelling, 37, 27–38, 2012).

Radius of gyration (Rg) of Hsp90 and Hsp90-taxifolin complex were analyzed to determine the effect of taxifolin on the folding of Hsp90. Rg value of complexes was found nearly same with continuous up and down during simulation (Fig. 4.18A). To identify the flexible regions of the protein, Root Mean Square Fluctuation (RMSF) of backbone residues from its time averaged position was analyzed. Taxifolin inbound

form showed markedly higher fluctuations as compared to unbound form (Fig. 4.18B)

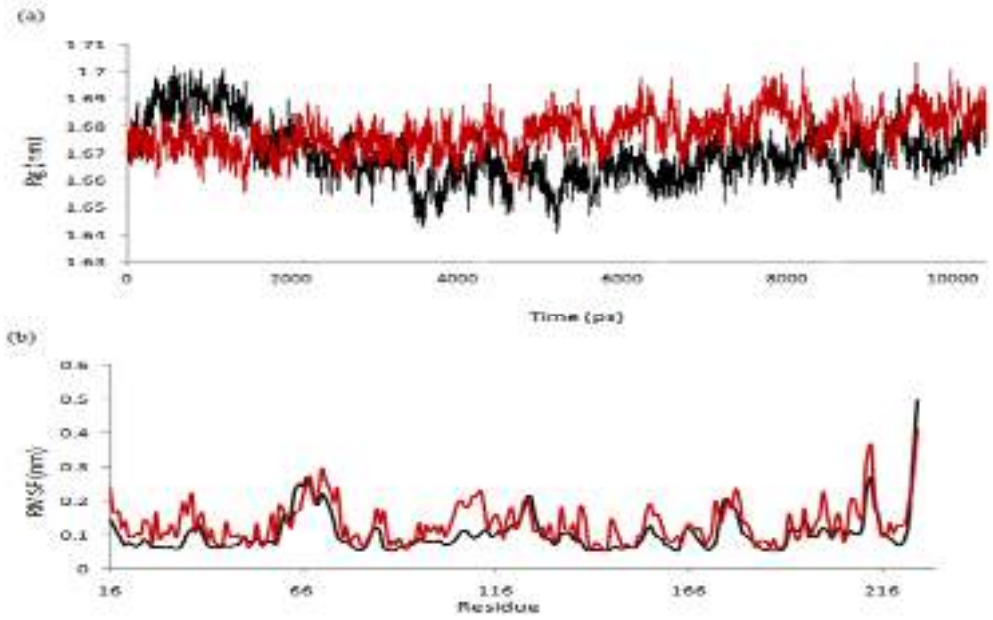

Fig. 4.18 (A) Radius of gyration of Hsp90 unbound (black) and Hsp90–taxifolin complex (red), (B) RMSF of Hsp90 backbone (black) and Hsp90–taxifolin backbone (red) **(**Published in Verma et al., Journal of Molecular Graphics and Modelling, 37, 27–38, 2012).

Several researchers have worked on targeted suppression of the ATPase activity of Hsp90 with small molecule inhibitors demonstrated anticancer activity in preclinical models and promising safety profile in humans (Janin, 2005; Vilenchik et al., 2004; Powers and Workman, 2007; Workman, 2003; Isaacs et al., 2003). Conformational coupling to the ATPase cycle requires N-terminal domain (NTD) dimerization for ATP hydrolysis and conformational transitions of a segment of the NTD structure known as the ‘‘ATP-lid’’. This segment is composed of two helices with the intervening loop located immediately adjacent to the ATP binding site (Ali et al.,

2006). The crystal structures of human Hsp90 NTD complexes with ADP (PDB id. 1BYQ) (Obermann et al., 1998) and geldanamycin (a known inhibitor of Hsp90, PDB id. 1YET) (Stebbins et al., 1997) have revealed that the ‘‘ATP-lid’’ segment projects out of the N-domain (‘‘open’’ or ‘‘lid-up’’ conformation) (Shiau et al., 2006; Richter et al., 2006). Ali et al., (2006) reported the crystal structure of the ATP-bound conformation Hsp90 NTD (PDB id. 2CG9) which showed that the lid segment of Hsp90 can be displaced from its position and folds over the nucleotide pocket to interact with the bound ATP (‘‘closed’’ or ‘‘lid-down’’ conformation) (Ali et al., 2006). Thus the ATPase cycle results in a structurally rigid conformational state of Hsp90 upon ATP binding, whereas on hydrolysis to ADP leads to a more structurally flexible state of Hsp90 (Shiau et al., 2006; Colombo et al., 2010; Terasawa et al., 2007). The conformational transition of the lid segment modulated by the inhibitor binding which stabilizes the open or lid-up conformation (Ali et al., 2006). The hydrolysis of ATP to ADP or binding with the active inhibitor leads to more relaxed and nonfunctional state of Hsp90 NTD. It is evident from MD simulation studies that taxifolin stabilized the open lid conformation of Hsp90 NTD. The loop of ‘‘ATP-lid’’ segment was pulled toward the taxifolin. A comparative investigation of ADP, geldanamycin and taxifolin bound Hsp90 NTD revealed the significant similarity in the overall structure (Fig. 4.19).

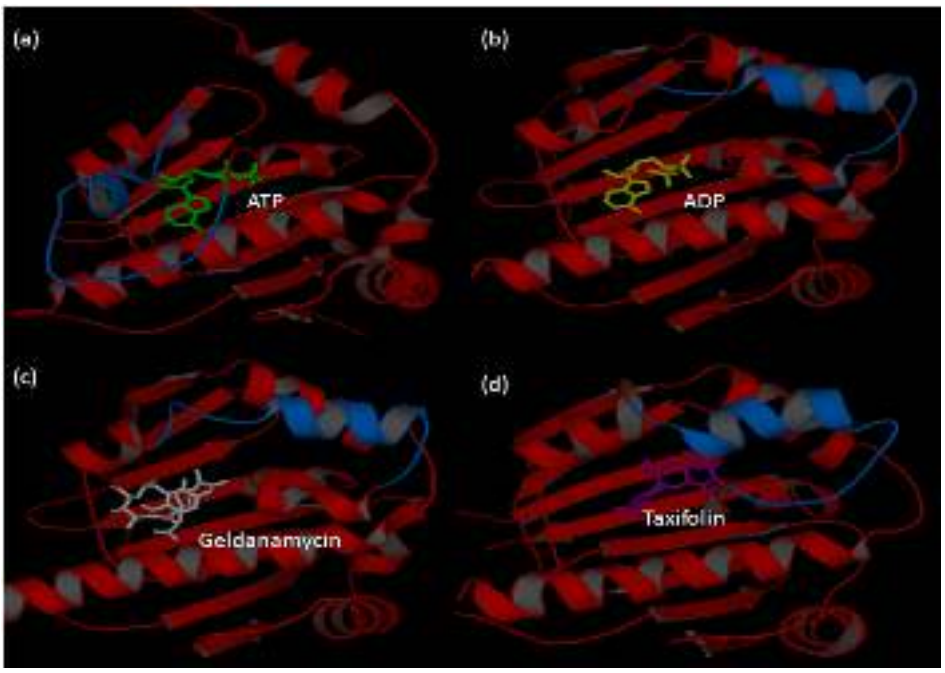

Fig. 4.19 (A) ATP bound "closed" or "lid-down" conformation of Hsp90 N-terminal domain, (B) ADP bound "open" or "lid-up" conformation of Hsp90 N-terminal domain, (C) Geldanamycin bound "open" or "lid-up" conformation of Hsp90 N-terminal domain, (D) Taxifolin bound "open" or "lid-up" conformation of Hsp90 N-terminal domain after10,000 ps MD simulation **(**Published in Verma et al., Journal of Molecular Graphics and Modelling, 37, 27–38, 2012)..

4.1.2.2 Approach 2: Interaction of taxifolin with Hsp90-Cdc37 complex

Hsp90 interacts with multiple co-chaperones to form a super-chaperone complex, including Cdc37, Aha1, p23/Sba1, Hop, Hsp70, and Hsp40 (Picard, 2002; Wegele et al., 2004; Reed, 1998). Each component in the complex has specific role associated with different types of protein. Cdc37, originally named as p50, was reported as an accessory factor to load the protein kinases to Hsp90 in the Hsp90 superchaperone complex (Smith et al., 2009; Pearl, 2005; Hunter and Poon, 1997). Silencing of Cdc37 reduces expression of a number of proteins such as ERBB2, CRAF, CDK4, CDK6, and phosphorylated AKT, which are highly relevant to cancer progression

(Zhang et al., 2008). Thus the involvement of the Hsp90-Cdc37 complex in the maturation and activity of oncogenic protein kinases makes the complex, a potential therapeutic target for cancer chemotherapy. Recently, a quinine methide triterpene compound Celastrol was shown to disrupt Hsp90/Cdc37 interaction and exhibited anticancer activity (Zhang et al., 2009; MacLean and Picard, 2003), which support the potential application of disrupting the protein/protein interaction of the Hsp90-Cdc37 complex for cancer therapy. Cdc37 is composed of the following three domains: a 15.5 kDa N-terminal domain (residues 1–127), a 16 kDa middle domain (residues 147–276), and a 10.5 kDa C-terminal domain (residues 283–378) (Shao et al., 2003; Roe et al., 2004). Cdc37 forms a complex with the N terminus of Hsp90 through its middle and C-terminal portions (Zhang et al., 2004; Sreeramulu et al., 2009). NMR mapping using human N-terminal Hsp90 (residues 18–223) and middle terminal Cdc37 (residues 147–276) fragments further showed a series of residues in the interaction patch, including Ser 113, Lys 116, Ala 117, Glu 120, Ala 121, Ala 124, Ala 126, Met 130, Gln 133, and Phe 134 of Hsp90 and His 161, Met 164, Leu 165, Arg 166, Arg 167, Asp 170, Trp 193, Ala 204, Leu 205, and Gln 208 of Cdc37 (Jiang et al., 2010; Grover et al., 2011).

To investigate probable role of taxifolin in disruption of the Hsp90-Cdc37 interaction, it was first examined whether taxifolin could bind residues at the interface of the Hsp90-Cdc37 complex. Molecular docking study revealed that taxifolin was interacted with Hsp90-Cdc37 interface residues with binding energy of -27.17 KJ/Mol. Taxifolin formed H-bond with the residues: His 210 of Hsp90 and

Lys 242 of Cdc37. For the confirmation of stability of taxifolin at Hsp90-Cdc37 complex interfaces and to study the dynamic changes at Hsp90-Cdc37 interface, molecular dynamic simulation was performed. Fig 4.20A showed that the RMSD profiles of backbone were always less than 0.3 nm for the entire simulation suggest the stability of simulation system.

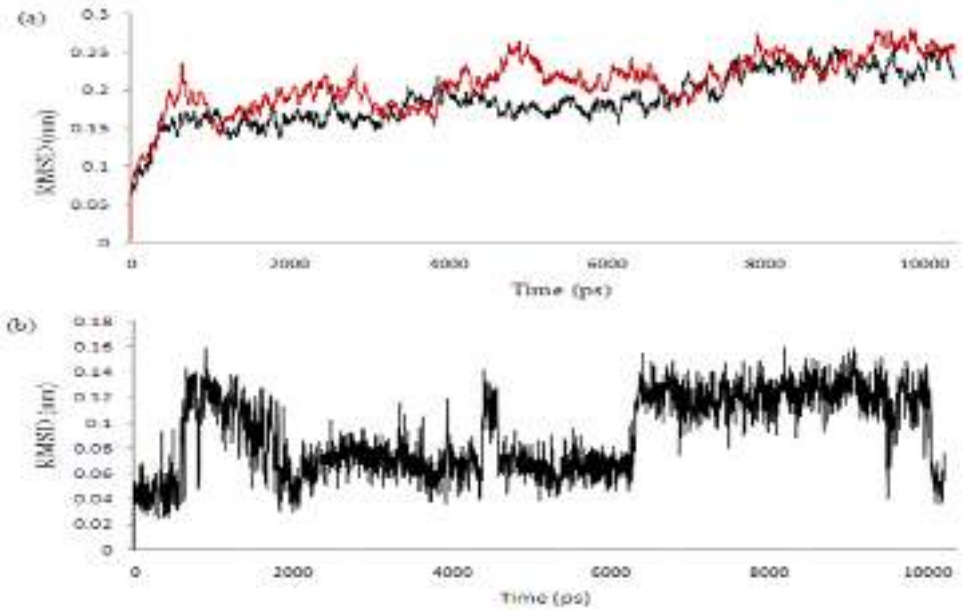

Fig. 4.20 (A) Plot of root mean square deviation (RMSD) of backbone of Hsp90–cdc37 unbound (black) and Hsp90–cdc37–taxifolin complex (red). (B) Plot of root mean square deviation (RMSD) of taxifolin **(**Published in Verma et al., Journal of Molecular Graphics and Modelling, 37, 27–38, 2012).

Taxifolin RMSD showed continuous fluctuations up to 0.16 nm throughout the MD simulation which suggests that significant domain movements were involved (Fig 4.20B). The adherence of the potential energy trajectories to more or less constant values for the Hsp90-Cdc37 complex and for the taxifolin docked complexes was observed during the entire simulation length (Fig 4.21A).

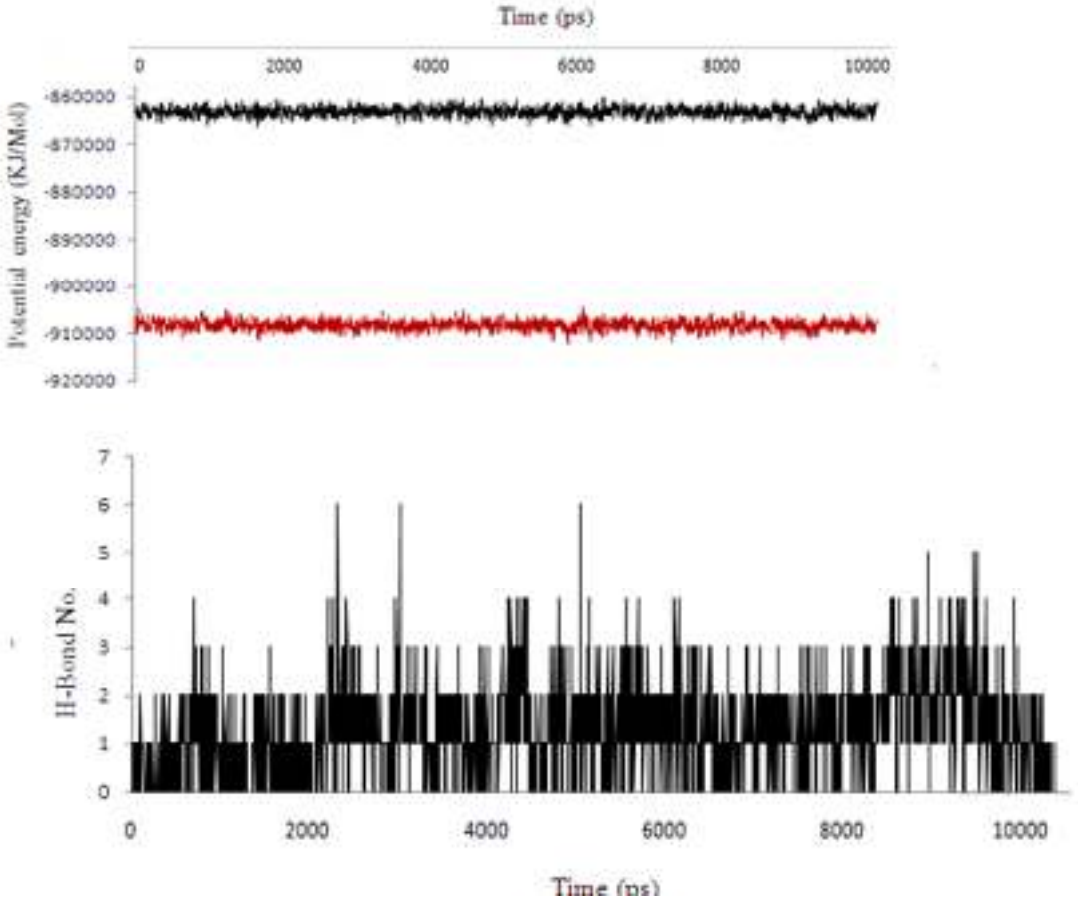

Fig. 4.21. (A) Potential energy profile of Hsp90–cdc37 unbound (black) and Hsp90–cdc37–taxifolin complex (red) during 10,000 ps MD simulation. (B) Number of H-bonds formed between taxifolin and Hsp90–cdc37 interface residues during 10,000 ps MD simulation **(**Published in Verma et al., Journal of Molecular Graphics and Modelling, 37, 27–38, 2012).

The energy values of the taxifolin bound complex were much lowered than that of the Hsp90-Cdc37 complex, indicating the thermodynamic stability of the ternary complex (Grover et al., 2010; Amadei et al., 1993; Grover et al., 2011). Number of H-bonds (cut off 0.35 nm) which were formed during MD simulation between taxifolin and Hsp90-Cdc37 complex interfaces was also calculated. A variable profile was observed which fluctuate between 0 to 6 with an average value of 1.24 (Fig 4.21B). 2D plots at the different time of simulation revealed that side chain of residue

Tyr 216 of Hsp90 and Lys 242 of Cdc37 involved in π-π and cation-π interaction with aromatic ring of taxifolin respectively (Fig 4.22).

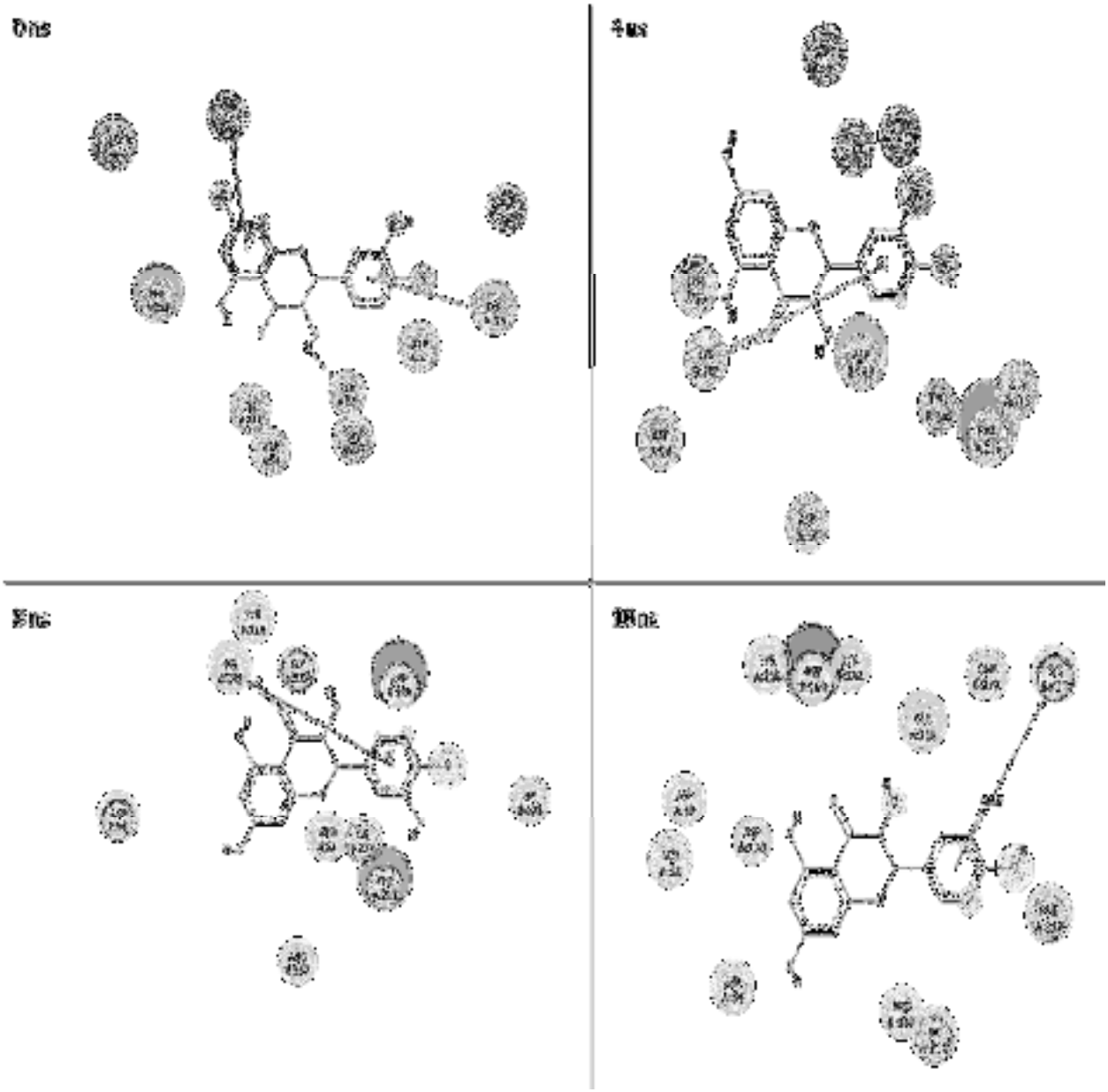

Fig. 4.22 2D plots of interaction between taxifolin and Hsp90–cdc37 complex at different time interval of MD simulation (Published in Verma et al., Journal of Molecular Graphics and Modelling, 37, 27–38, 2012).

The simulation length used in this study was found to be enough to allow rearrangement of side chains of the native as well as the drug complexed proteins to

find their most stable binding mode. To identify the flexible regions of the protein, RMSF of backbone from its time averaged position was analyzed. The RMSF profile of residue backbone revealed slight higher fluctuation in taxifolin bound complex as compared to unbound form during the course of simulation. This suggests that binding of taxifolin makes backbone more flexible to move. Further, the flexibility of Hsp90 backbone was found more as compared to Cdc37. This might be due to the restriction caused by interaction of taxifolin to Cdc37 (Fig 4.23).

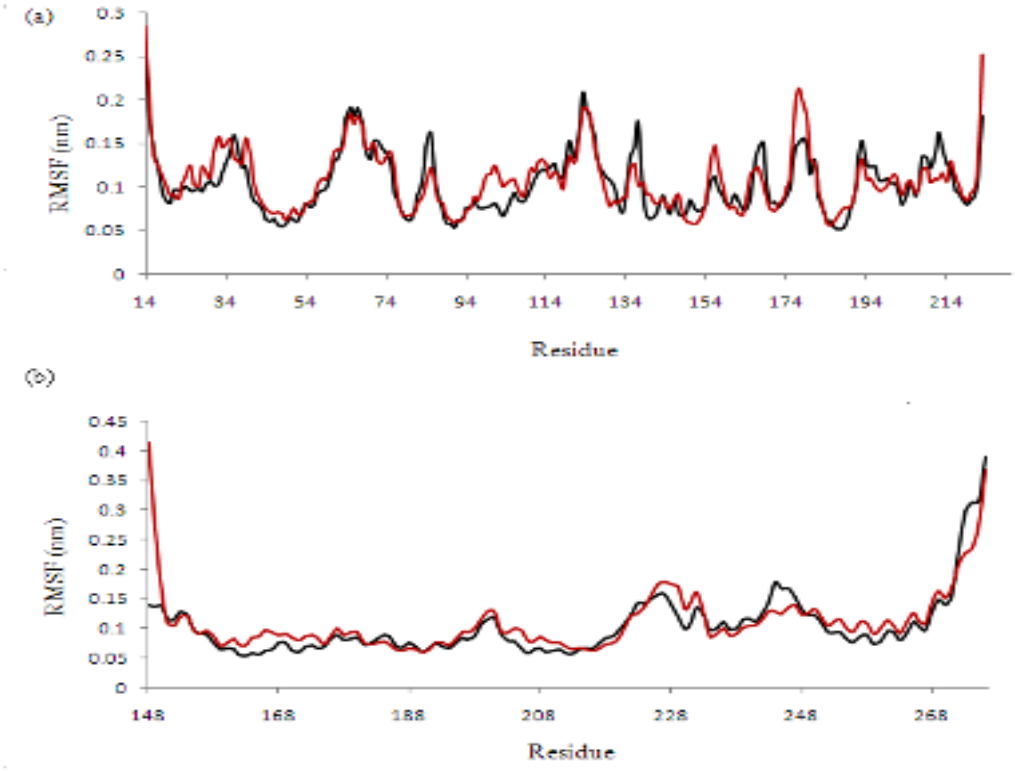

Fig. 4.23. (A) RMSF of Hsp90 residues backbone (black) in Hsp90–cdc37 complex (taxifolin unbound) and Hsp90 residues backbone (red) in Hsp90–cdc37 complex (taxifolin bound), (B) RMSF of Cdc37 residues backbone (black) in Hsp90–cdc37 complex (taxifolin unbound) and Cdc37 residues backbone (red) in Hsp90–cdc37 complex (taxifolin bound) **(**Published in Verma et al., Journal of Molecular Graphics and Modelling, 37, 27–38, 2012).

The RMSF profile of critically required interface residue side chains (involved in

complex formation) suggested higher fluctuation in taxifolin bound complex as compared to unbound form throughout MD simulation study (Fig 4.24).

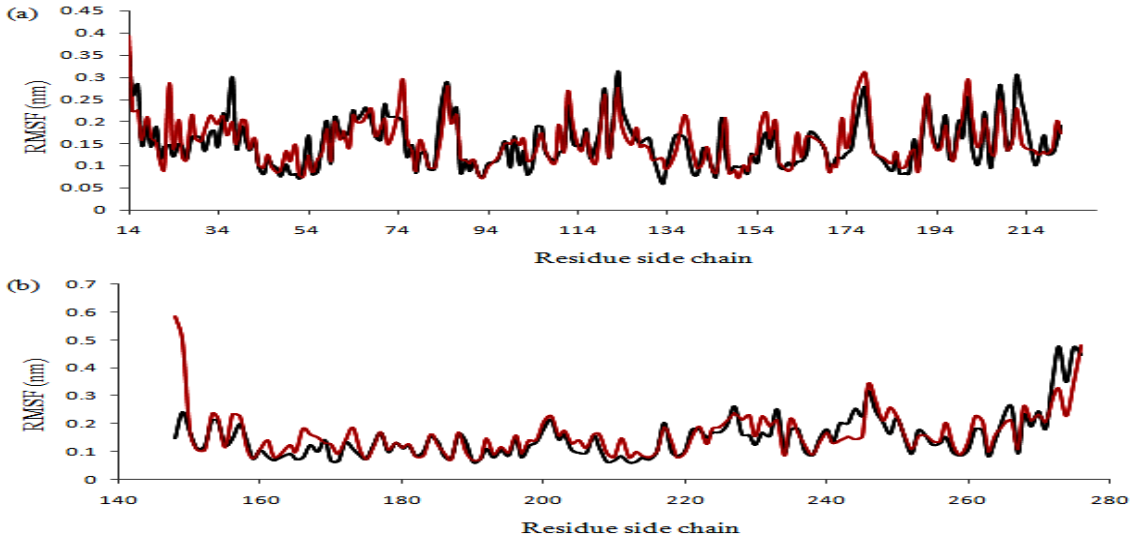

Fig. 4.24 (A) RMSF of Hsp90 residue side chains (black) in Hsp90–cdc37 complex (taxifolin unbound) and Hsp90 residue side chains (red) in Hsp90–cdc37 complex (taxifolin bound), (B) RMSF of Cdc37 residue side chains (black) in Hsp90–cdc37 complex (taxifolin unbound) and Cdc37 residue side chains (red) in Hsp90–cdc37 complex (taxifolin bound) **(**Published in Verma et al., Journal of Molecular Graphics and Modelling, 37, 27–38, 2012).

These results suggested that binding of taxifolin made these residues either structurally unrestricted or disruption of stable interactions at the interface.

In a recent study Jiang et al. reported that mutations in Hsp90 (Q133A, F134A, and A121N) and mutations in Cdc37 (M164A, R167A, L205A, and Q208A) reduced the Hsp90–cdc37 interaction by 70–95% as measured by the resorted luciferase activity through Hsp90–cdc37-assisted complementation (Jiang et al., 2010). Mutations in Hsp90 (E47A and S113A) and a mutation in Cdc37 (A204E) decreased the Hsp90–cdc37 interaction by 50%. In contrast, mutations of Hsp90 (R46A, S50A, C481A,

and C598A) and Cdc37 (C54S, C57S, and C64S) did not change Hsp90–cdc37 interactions (Jiang et al., 2010). Single amino acid mutation in the interface of Hsp90–cdc37 is sufficient to disrupt the interaction, although Hsp90–cdc37 interactions are through large regions of hydrophobic and polar interactions (Jiang et al., 2010). These findings revealed the importance of some specific residues critically required for complex formation. During simulation studies we found that taxifolin binding to Hsp90–cdc37 complex disrupt the key interaction required for functional complex formation. A strong interaction between Glu 47 of Hsp90 and Arg167 of Cdc37 bridged by water molecule was vanished in presence of taxifolin (Fig. 4.25A and C). Gln 133 of Hsp90 showed polar interaction with Arg166 and Arg167 of Cdc37 during MD simulation of taxifolin unbound form. This interaction significantly contributes to complex formation (Jiang et al., 2010). Binding of taxifolin to Hsp90–cdc37 complex disrupt this interaction as evidenced by MD simulation (Fig. 4.25B and D).

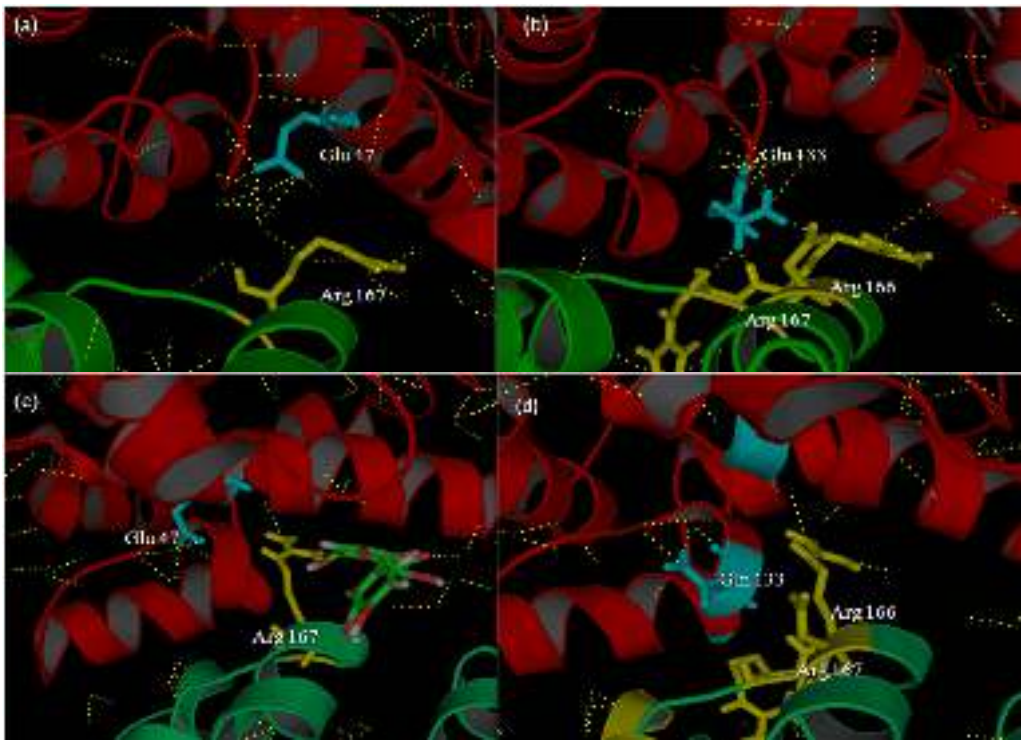

Fig. 4.25. (A) Interaction between Arg167 of Cdc37 and Glu 47 of Hsp90 in taxifolin unbound form, (B) Interaction between Arg166 and, Arg167 of Cdc37 and Gln133 of Hsp90 in taxifolin unbound form, (C) Disruption of interaction between Arg167 of Cdc37 and Glu 47 of Hsp90 in taxifolin bound form, (D) Disruption of interaction between Arg166 and, Arg167 of Cdc37 and Gln133 of Hsp90 in taxifolin bound form **(**Published in Verma et al., Journal of Molecular Graphics and Modelling, 37, 27–38, 2012).

A network of polar contact was found Lys 116 and Glu 120 of Hsp90 with peptide bond (CONH) of Ala 204 and Leu 205 of Cdc37 (Fig. 4.26) which was vanished in presence of taxifolin (Fig. 4.26A and B). In taxifolin unbound complex Gln 133 of Hsp90 also found to form H-bond with Asp 170 of Cdc37 which was found absent in taxifolin bound form (Fig. 4.26C and D).

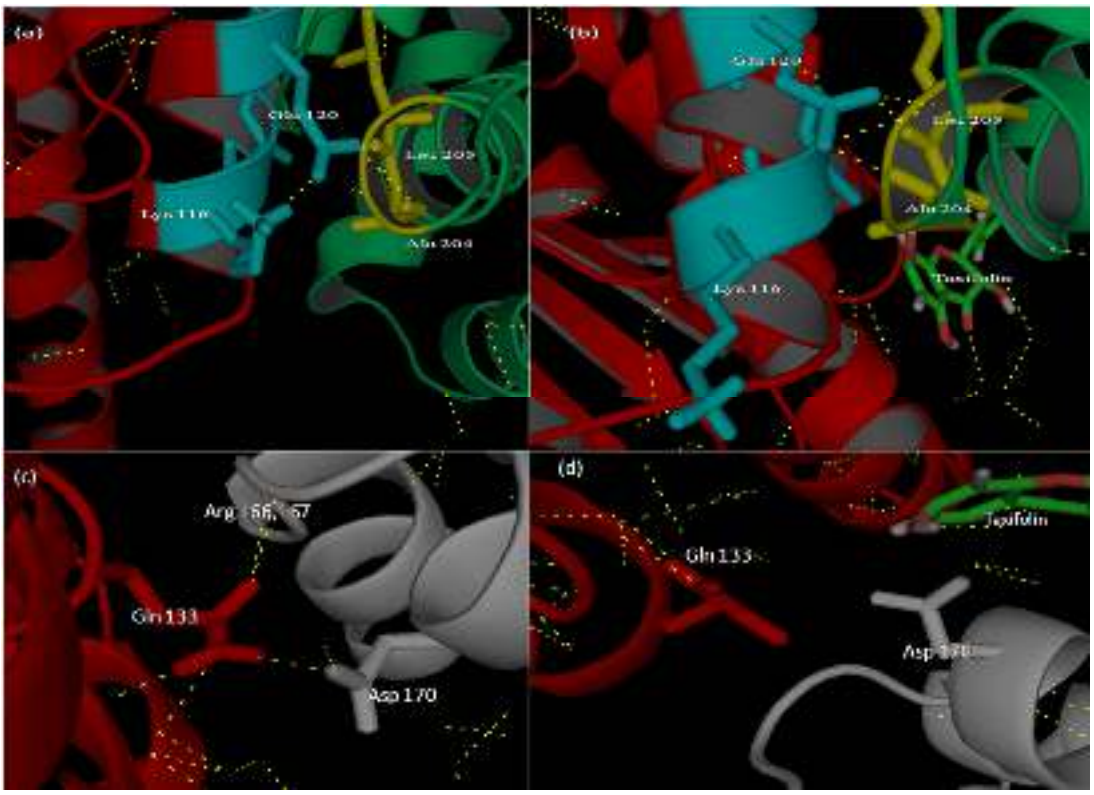

Fig. 4.26. (A) Interaction between Ala 204, and Leu 205 of Cdc37 and Lys 116, and Glu 120 of Hsp90 in taxifolin unbound form, (B) Interaction between Ala 204 and, Leu 205 of Cdc37 and Lys 116, and Glu 120of Hsp90 in taxifolin bound form, (C) Interaction between Asp 170 of Cdc37 and Gln 133 of Hsp90 in taxifolin unbound form, (D) Disrupted interaction between Asp 170 of Cdc37 and Gln 133 of Hsp90 in taxifolin bound form **(**Published in Verma et al., Journal of Molecular Graphics and Modelling, 37, 27–38, 2012).

These results showed that taxifolin interrupt the residue interaction between Hsp90 and Cdc37 which are critically required for active complex formation. Thus, the taxifolin when bound to ATP binding site of Hsp90 prevented the dimerization by disrupting ATPase cycle. On the other hand, on binding to Hsp90–cdc37 interface, it disrupted the interaction between the interface residues of Hsp90 and Cdc37, which were found to play critical role in the formation of superchaperone complex.

4.1.3 Molecular target 3: Mouse double minute 2 (MDM2)

4.1.3.1 Approach 1

Molecular docking results revealed that quercetin and taxifolin bound to hydrophobic groove of MDM2 with binding energy -28.56 and -30.66 Kj/mol respectively (Fig. 4.27A, B). Quercetin showed hydrogen bonding with Gly 16, Ser 17, Phe 55 and Val 93 along with π- π interaction with His96 and π-sigma with Phe 55. Taxifolin showed similar interaction as quercetin except π-sigma interaction with Phe 55.

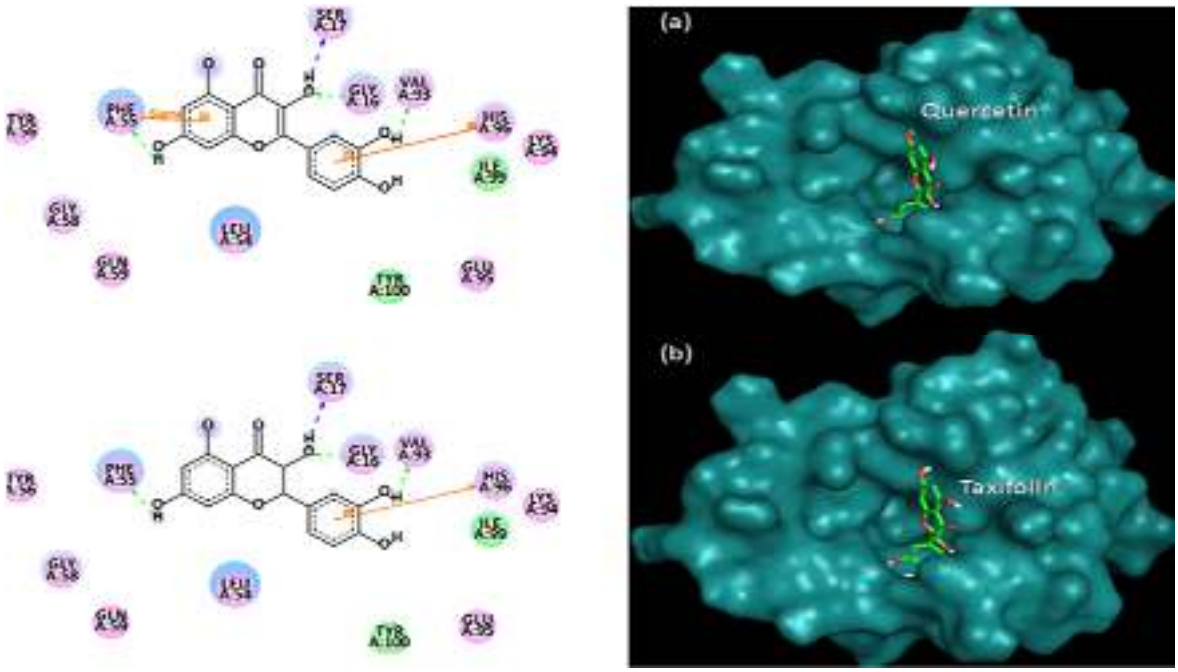

Fig. 4.27. (A) Quercetin bound to hydrophobic groove of MDM2 and 2D presentation of interaction with residues, (B) Taxifolin bound to hydrophobic groove of MDM2 and 2D presentation of interaction with residues (Verma et al., Molecular Informatics, 32,203-212, 2013**)**.

The lowest binding energy (most negative) docking conformation generated by Autodock was taken as initial conformation for MD simulation. Fig. 4.28A

showed that the RMSD profiles were always less than 0.25 nm for both quercetin and taxifolin bound MDM2 backbone during the entire simulation suggesting the suitability of MD simulation run for post analysis. Fig. 4.28B showed the RMSD profile of ligands bound to MDM2 pocket. Quercetin and taxifolin showed stable profile throughout the simulation. These results showed the stable binding of ligands in the hydrophobic pocket of MDM2.

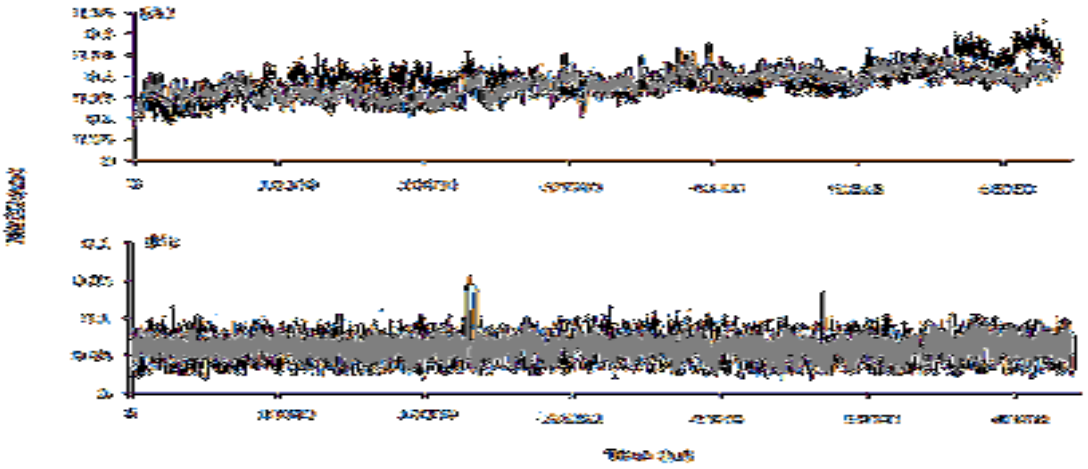

Fig. 4.28. (A) Plot of root mean square deviation (RMSD) of backbone of MDM2 complexed with quercetin (black) and with taxifolin (grey), (B) Plot of root mean square deviation (RMSD) of quercetin (black) and taxifolin (grey) in hydrophobic groove of MDM2 (Verma et al., Molecular Informatics, 32,203-212, 2013**)**.

Comparative analysis of final pose of MDM2-ligand complex after 65 ns molecular dynamics simulation with crystal structure of MDM2 revealed that binding of the quercetin and taxifolin bring significant conformational changes in the MDM2 structure. Fig. 4.29 clearly indicates the distortion of hydrophobic groove in the ligand bound MDM2. However quercetin showed higher effect on the groove and found to be completely overlapped by N-terminal loop in quercetin bound MDM2. All these results indicate that these polyphenols have potential to inhibit the MDM2

binding with p53 by occupying and distorting structure of hydrophobic groove. The binding pocket, although well defined in apo MDM2, undergoes profound conformational changes upon ligand binding (Uhrinova et al., 2005; Kuttner and Engel, 2012; Allen et al., 2009). The structure of MDM2 complexed to a small molecule inhibitor of MDM2–p53 interaction, chromenotriazolopyrimidine (PDB: 3JZK) (Allen et al., 2009), demonstrates that the compound and the p53 peptide share the same binding cavity and induce similar conformation changes upon binding. These previous studies further support the inhibitory potential of quercetin and taxifolin. These polyphenols stabily occupied the p53 binding site similar to chromeno-triazolopyrimidine (Fig. 4.34).

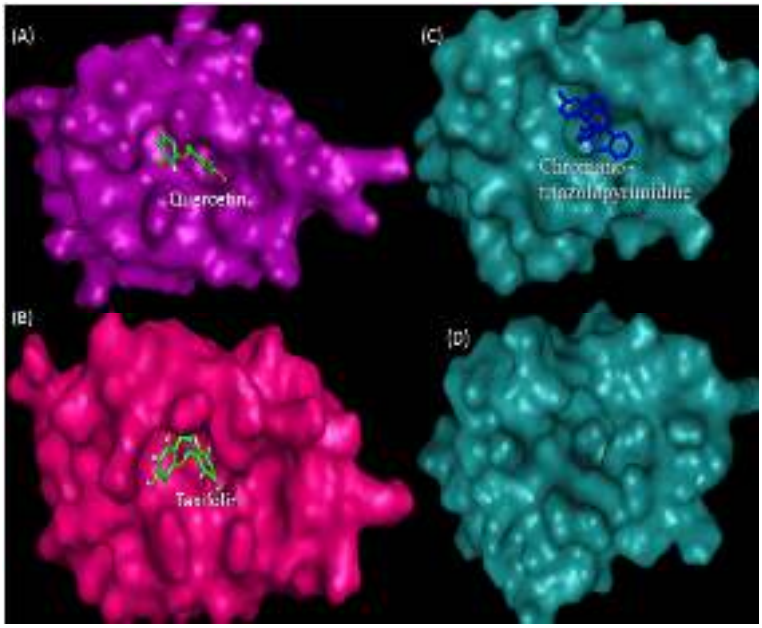

Fig. 4.29. Comparison of last pose of 65 ns MD simulation of MDM2 in ligands bound form with apo and chromeno-triazolopyrimidine complexed MDM2 (Verma et al., Molecular Informatics, 32,203-212, 2013).

Further 2D plots (Discovery Studio Modeling Environment , 2011) of interaction of

final pose of 65 ns MD simulation was generated and compared with chromeno-triazolopyrimidine and another inhibitor benzodiazepine (Grasberger et al, 2005). It was found that binding pattern of quercetin and taxifolin was very similar to the both known inhibitors as shown in Fig 4.30.

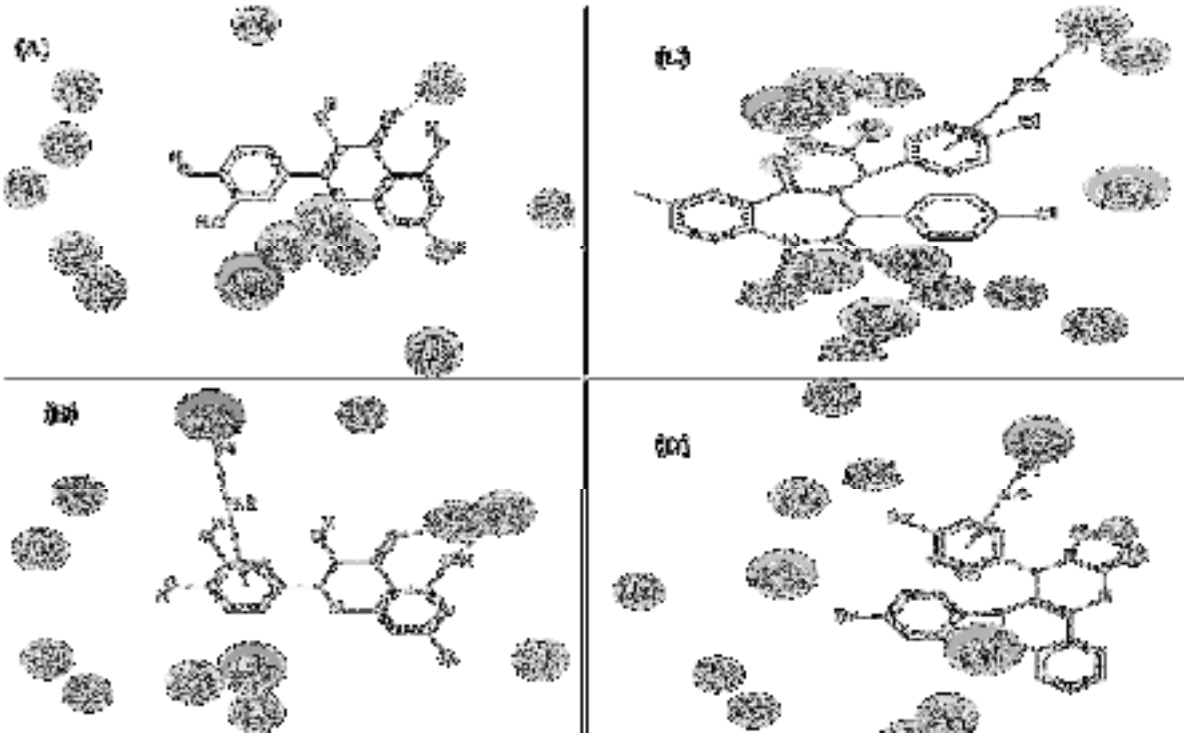

Fig. 4.30. Comparison of interaction of last pose of 65 ns MD simulation of MDM2 with ligands and benzodiazepine, and chromeno-triazolopyrimidine complexed MDM2 (Verma et al., Molecular Informatics, 32,203-212, 2013**)**.

In addition, the total binding free energy for the MDM2-ligand complexes and their detailed energy contributions calculated according to the MM-PBSA approach, are summarized in Table 4.1. The ΔG_{bind} can be divided into polar (ΔGele,sol +ΔEele) and nonpolar energies ($\Delta G_{nonpolar} + \Delta E_{vdw}$). The free energy of quercetin and taxifolin binding to MDM2 is primarily derived from the $\Delta G_{nonpolar} + \Delta E_{vdw}$, while the $\Delta G_{ele,sol}$

+ ΔE_{ele} shows a likely unfavorable contribution. This is due to the intermolecular van der Waals energies, which is mainly achieved from the ligand binding residues. These results suggest that quercetin and taxifolin can bind to MDM2, dominantly, through van der Waals energy. As compared to previously known inhibitors (Chen et al., 2011), quercetin and taxifolin showed remarkable similarity in binding pattern and affinity for the hydrophobic groove of MDM2.

Table 4.1. Calculated energy components, binding free energy (kcal/mol) of quercetin and taxifolin binding to MDM2.

Energy components (kcal mol^{-1})	Quercetin	Taxifolin
ΔE_{ele}	-28.07	-39.17
ΔE_{vdw}	-196.71	-185.66
ΔE_{MM}	-224.78	-224.83
$\Delta G_{ele,sol}$	197.65	195.57
$\Delta G_{nonpolar,sol}$	-8.7	-10.3
ΔG_{sol}	188.95	185.27
$-T\Delta S$	-22.80	-23.71
$\Delta G_{bind\ (predicted)}$	-13.03	-15.85

4.1.3.2 Approach 2

Taxifolin and quercetin were found to bind at interface of MDM2-P53 complex with lowest binding energy -34.52 Kj/mol and -34.81 Kj/mol respectively. These results indicate that both ligands have high affinity for the MDM2-P53 interface. The major interactions shown in the MDM2-p53 interface are the important H-bonds with

residues Lys 24 and, Leu 26 of p53 and Tyr 51 and, Gln 55 of MDM2. The groups involved in H-bonding were hydroxyl (hydrogen donar) and carbonyl (hydrogen acceptor) group of taxifolin and quercetin.

The MDM2-p53-taxifolin and MDM2-p53-quercetin complex with the binding energy of -34.52 Kj/mol and -34.81 Kj/mol, respectively, obtained using Autodock was used for carrying out MD simulation. Fig. 6a shows that the RMSD trajectory was always less than 0.25 nm up to ~7000 ps for taxifolin bound form. A high rise in the RMSD was observed at ~ 7500 ps and subsequently a constant profile was observed with up and down for very small time intervals. This increase in RMSD was found to be in the good agreement with the snapshots recorded at and after 7500 ps (described later) which revealed the separation of p53 segment with MDM2. Analysis of taxifolin RMSD indicates that taxifolin showed remarkable stability at interface of MDM2-p53 complex during MD simulation. However, some high fluctuations were during the simulation (Fig. 4.31B). In quercetin bound form, the RMSD trajectories of backbone showed high increase from the value of 0.25 nm after ~10000 ps and subsequently a more or less constant profile was observed (Fig. 4.31A).

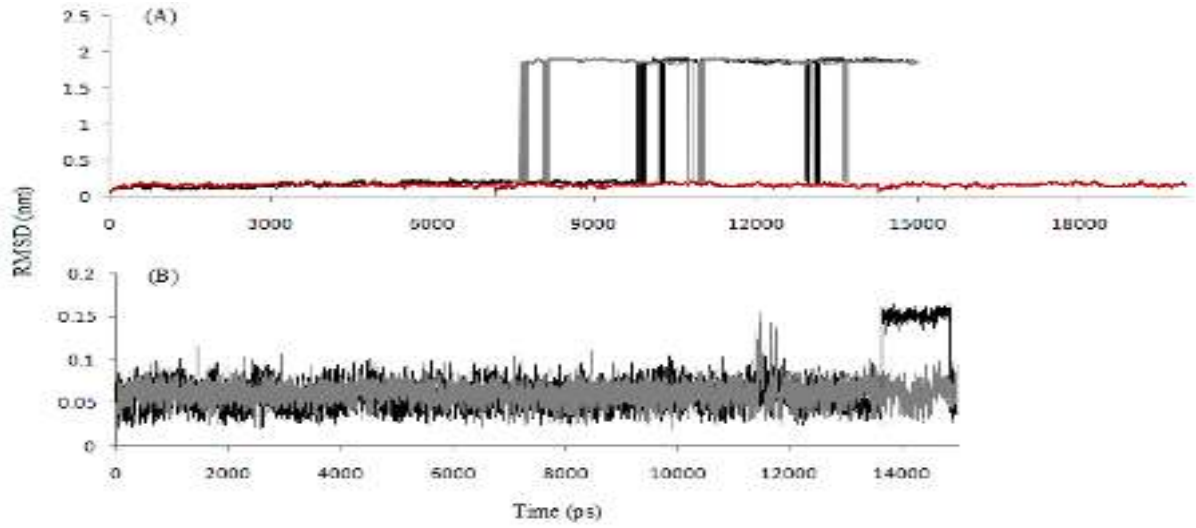

Fig. 4.31. (A) Plot of root mean square deviation (RMSD) of backbone of MDM2-p53 complexed with taxifolin (grey), MDM2-p53 complexed with quercetin (black) and without ligand (red), (B) Plot of root mean square deviation (RMSD) of taxifolin (grey) and quercetin (black) (Verma et al., Molecular Informatics, 32,203-212, 2013).

Similar to taxifolin, this increase of RMSD was found to be associated with the dissociation of MDM2-p53 complex (described later). Analysis of quercetin RMSD indicated that quercetin showed stability at interface of MDM2-p53 complex during MD simulation. However, increase in RMSD was observed after ~ 13000 ps (Fig 4.35B). This increase in RMSD indicates the dissociation of quercetin along with p53. MDM2-p53 complex in absence of any ligand showed stability as compared to ligand bound complex (Fig 6a). Previously, Espinoza-Fonseca and García-Machorro (2008) showed the stability of MDM2-p53 complex during a long MD simulation using same PDB structure (Espinoza-Fonseca and García-Machorro, 2008).

Number of H-bonds (cut off 0.35 nm) which were formed during MD simulation between ligands and MDM2-p53 was also calculated. A variable profile was observed which fluctuate between 0 to 3 with an average value of 0.15 and, 0 to 4

with average value 0.25 for taxifolin and quercetin respectively (Fig. 4.32).

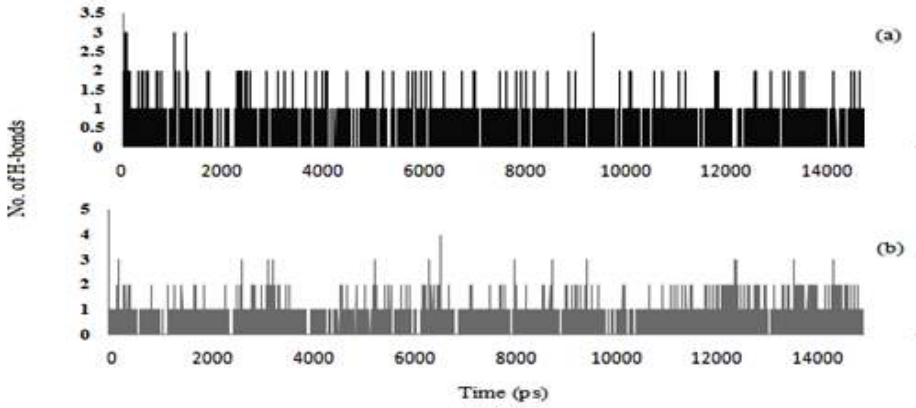

Fig. 4.32. (A) Number of H-bonds formed between taxifolin and MDM2-p53 interface residues, (B) Number of H-bonds formed between quercetin and MDM2-p53 interface residues during 12 000 ps MD simulation (Verma et al., Molecular Informatics, 32,203-212, 2013**)**.

Furthermore, to identify the flexible residues of the protein, Root Mean Square Fluctuation (RMSF) of backbone atoms from its time averaged position was analyzed. All the residues of both MDM2 and p53 showed marked higher fluctuation in taxifolin and quercetin bound forms as compared to unbound form. The p53 residues showed higher fluctuation increased by ~1nm as compared to ligand unbound form (Fig. 4.33). This profile confirmed that ligand binding induced movement in the residues of protein complex.

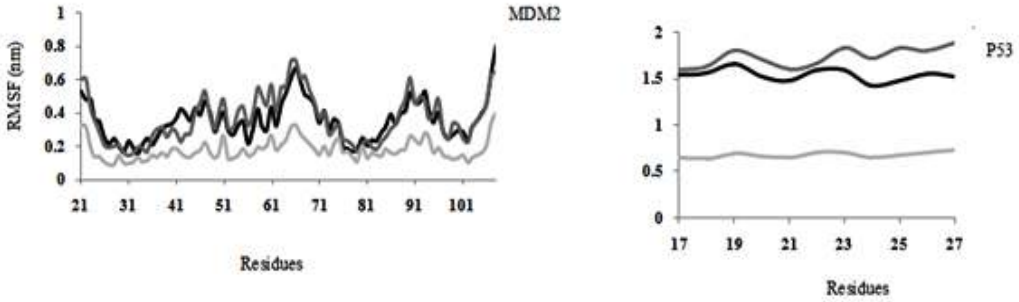

Fig. 4.33. RMSF of MDM2-p53 residues backbone in taxifolin bound (black), quercetin bound (grey) and ligand unbound form (light grey) (Verma et al., Molecular Informatics, 32,203-212, 2013**)**.

Coordinates of the MDM2-p53-taxifolin system recorded at different time interval of simulation revealed that binding of the MDM2-p53 remained intact for ~7000 ps. thereafter, p53 segment detached from the MDM2 cleft as observed in the 12000 ps and final 14000 ps snapshots (Fig. 4.34).

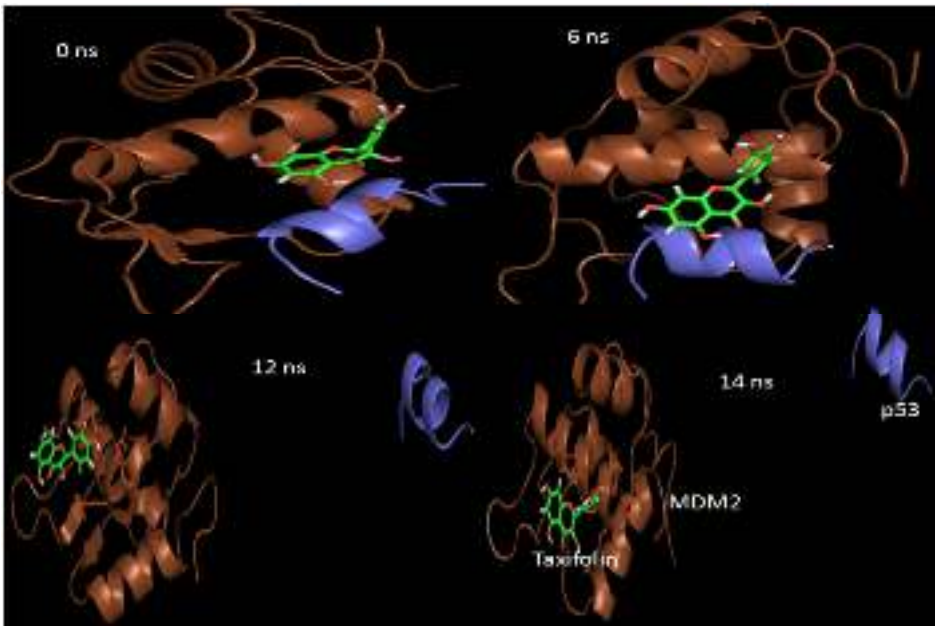

Fig 4.34. Snap shots at different time interval of MDM2-p53 complexed with taxifolin for 15 000 ps MD simulation showing dissociation of complex (Verma et al., Molecular Informatics, 32,203-212, 2013**)**.

These results were favored by the RMSD and RMSF profile described earlier. In case of MDM2-p53-quercetin major changes were observed ~10 ns. p53 segment along with quercetin leave the MDM2 binding site as observed in 14 ns snapshot while at 12 ns quercetin was found bound to MDM2 (Fig. 4.35).

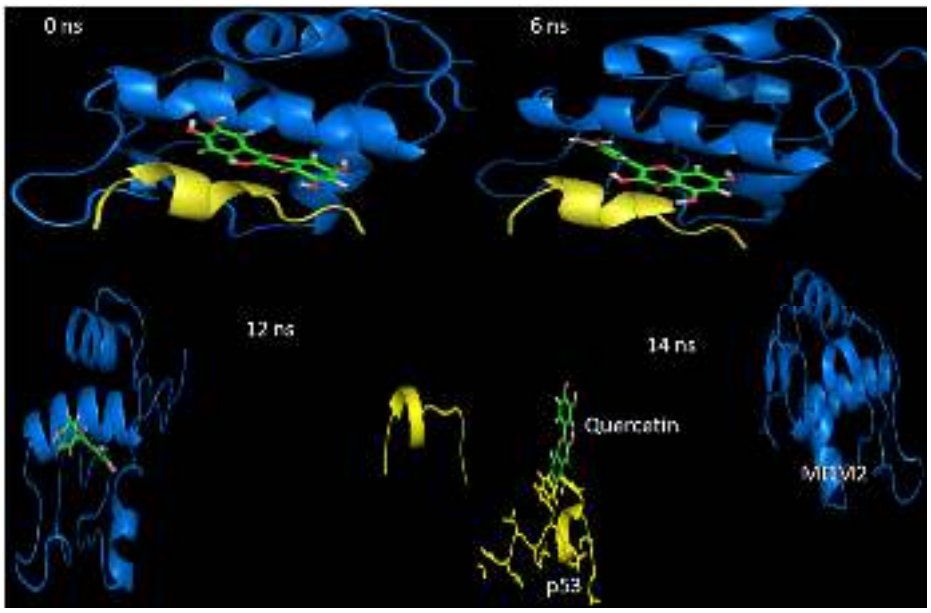

Fig 4.35. Snap shots at different time interval of MDM2-p53 complexed with quercetin for 15 000 ps MD simulation showing dissociation of complex (Verma et al., Molecular Informatics, 32,203-212, 2013**)**.

Analysis of the MDM2-p53 complex (without ligand) during simulation revealed that only few residues contribute to the interaction of these two proteins. Phe 19, Trp 23 and Leu 26 of P53 were the residues which oriented toward the MDM2 binding cleft. The importance of these residues was previously described several times.[5,36] In case MDM2 Lys 47, Tyr 51, Gln 55 and Met 58 were found critical residues involved in interaction with p53. The interaction of these two proteins is mainly dependent on the hydrophobic interactions (Chen et al., 2011; Allen et al., 2009). To found the effect of ligands on these residues, we analyzed snapshots of simulation at different time interval. The 2D plot of taxifolin and MDM2-p53 interaction at different time interval of MD simulation showed and confirmed that the hydrophobic interactions were dominated during simulation. Initially, taxifolin showed π-π interaction with both MDM2 and p53 which finally, completely, switched to π-π and, cation-π

interaction between taxifolin aromatic ring A and Tyr 51 and, Lys 47 respectively (Fig. 4.36).

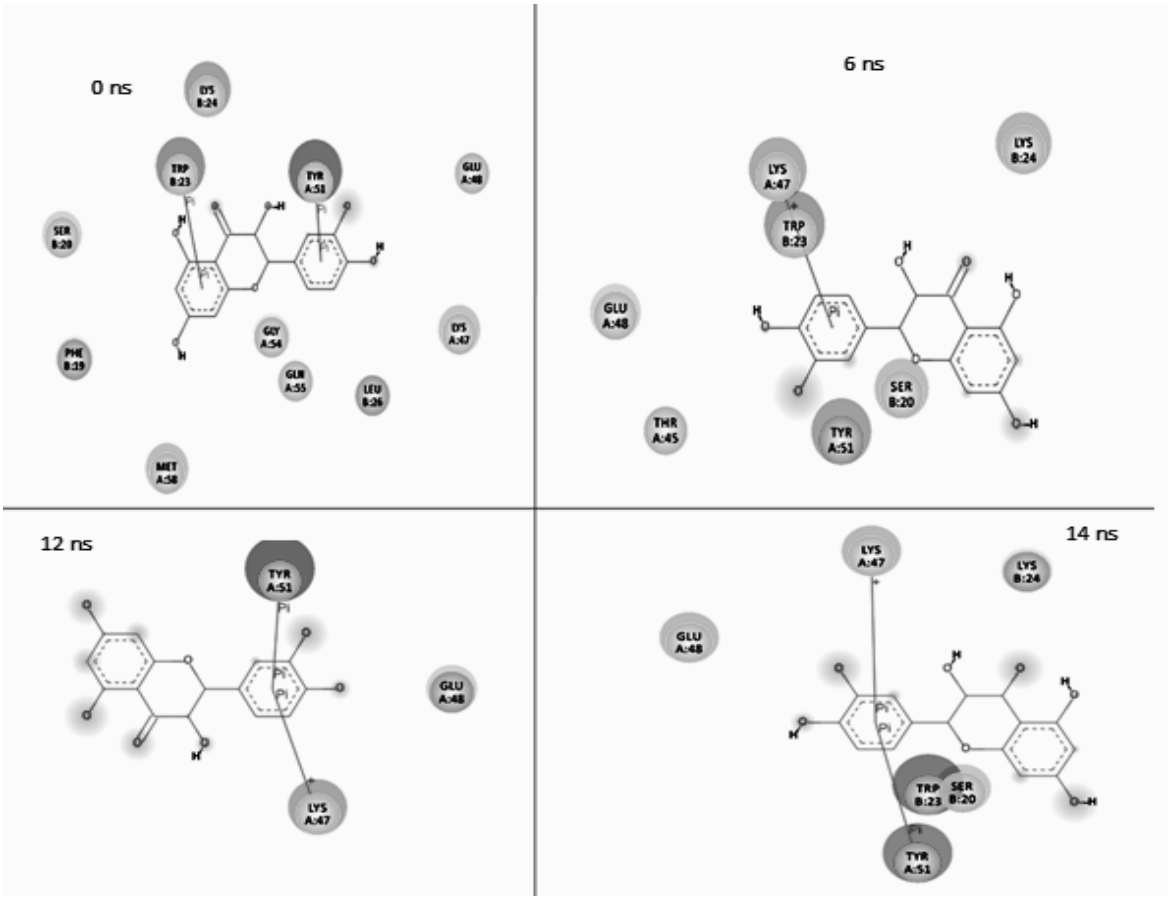

Fig 4.36 2D plots of interaction between taxifolin and MDM2-p53 at different time interval of 15 000 ps MD simulation (Verma et al., Molecular Informatics, 32,203-212, 2013).

In this way interaction of Trp 23 of p53 and Tyr 51 of MDM2 transformed into Trp 23-B-C ring and, Tyr 51-A ring interaction and finally in to A ring of taxifolin and Tyr 51and, Lys 47 of MDM2. The 2D plot of quercetin and MDM2-p53 interaction also showed that initially, quercetin involved in π-π interaction with MDM2 by C ring. At 12000 ps B and, C-ring of quercetin found in π-π interaction wirh Tyr 51(Fig.

4.37).

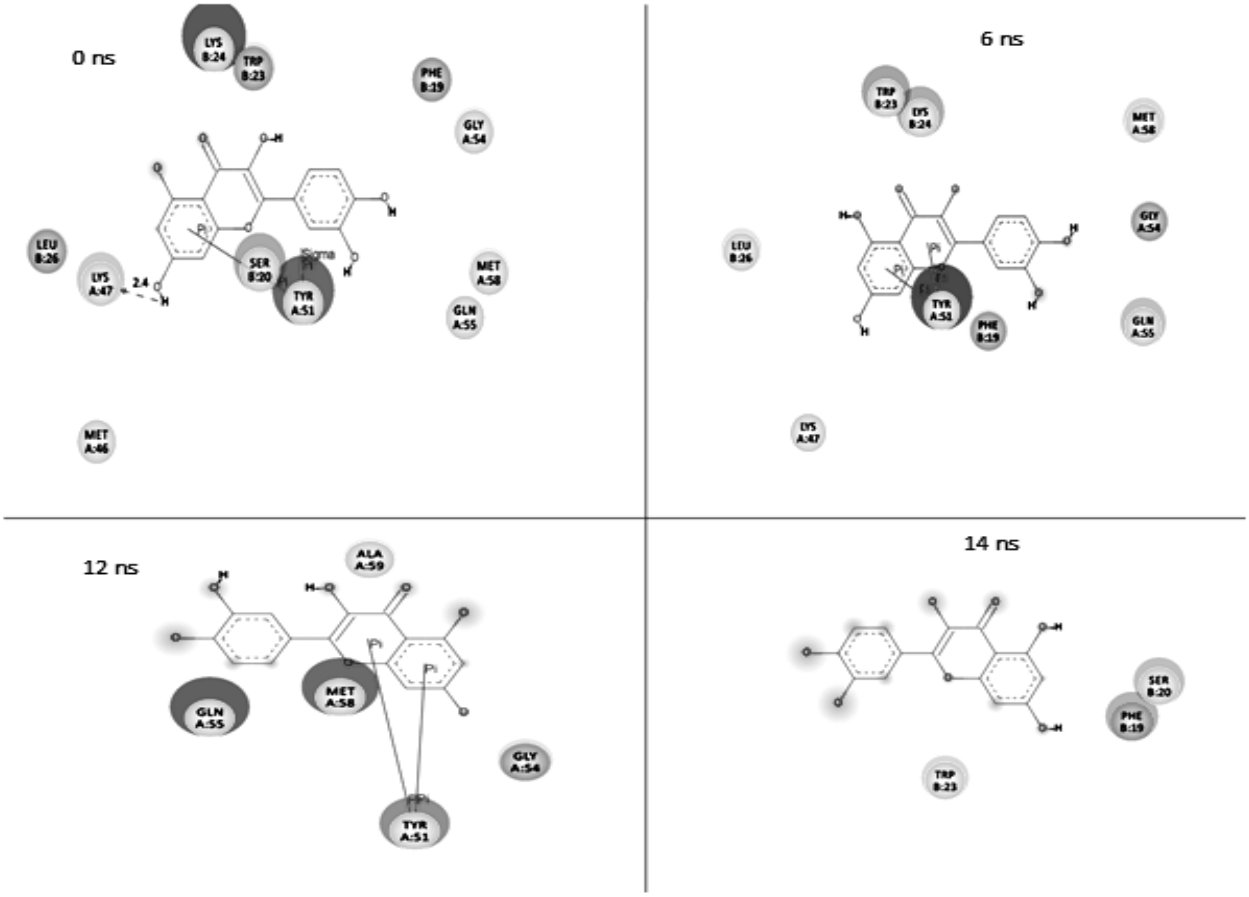

Fig 4.37. 2D plots of interaction between quercetin and MDM2-p53 at different time interval of 15 000 ps MD simulation (Verma et al., Molecular Informatics, 32,203-212, 2013).

It is well established that interaction of MDM2 and p53 is governed by hydrophobic groups of residues. The presence of aromatic groups in the ligands was found be the main reason behind the masking of the interaction between proteins. Further, Tyr 51 residue was found to play lead role in interaction with p53 as the masking of Tyr 51 hydrophobic side chain by ligands led to separation of p53. Both approaches used in the study were found to be supported by each other. Being natural polyphenols, antioxidant and presence in large number of fruits, vegetables and beverages, these

polyphenols may be used as lead compound for cancer prevention.

4.1.4 Molecular target 4: Vascular epithelial growth factor receptor 2 (VEGFR-2) kinase

Taxifolin was found to bind at ATP-binding site of VEGFR-2 with lowest binding energy-8.30 Kcal/Mol (Fig. 1). Free energy of binding is calculated as a sum of four energy terms of intermolecular energy (vanderwaal, hydrogen bond, desolvation energy and electrostatic energy), total internal energy, torsional free energy and unbound system energy. The major interactions shown in the VEGFR-2 kinase-ATP-binding site are the important H-bonds with Leu 838 (2.86 Å), Glu 883 (2.77 Å, 2.69 Å), Glu 915 (2.72 Å) and Cys 917 (2.72 Å) (Fig. 4.38).

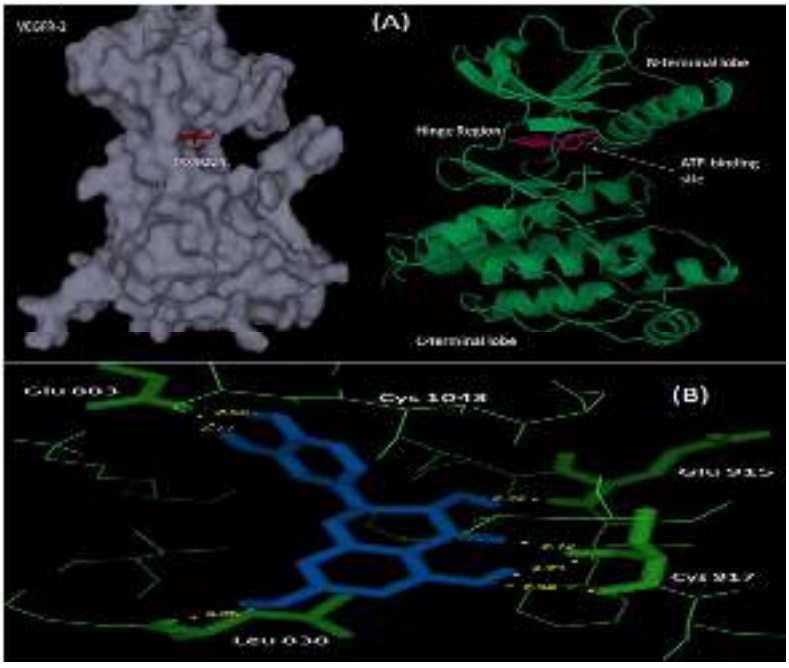

Fig. 4.38. (A) Bindinding of taxifolin at ATP-binding site on VEGFR-2 kinase: surface view and ribbon structure, (B) Stereo view of H-bond pattern of taxifolin with ATP-binding pocket residues (Verma et al., Journal of Applied Pharmaceutical Science, 2, 41-46, 2012).

Large negative binding energies of VEGFR-2-taxifolin complex were obtained by

Autodock 4.0 as is evident from Table1. The groups involved in H-bonding were hydroxyl (hydrogen donar), and carbonyl (hydrogen acceptor) group of taxifolin and NH (hydrogen donar) of Cys 917, and oxygen atoms (hydrogen acceptor) of side chain or backbone of residues. These results evidenced that taxifolin has very high affinity for the ATP-binding site of VEGFR-2.

The VEGFR-2 kinase-taxifolin complex with the binding energy of -8.32 kcal/mol obtained using Autodock was used for carrying out MD simulation. After MD simulation, we calculated RMSD trajectory of backbone of VEGFR-2 kinase and VEGFR-2 kinase-taxifolin complex at every 0.5 ps by using its initial structure as a reference. Fig. 4.39 showed that the RMSD trajectories were always less than 3.0 Å (0.3 nm) for the entire simulation suggesting the stability of simulation system. The trajectories were stabilized after 500 ps till 3500 ps and thereafter slight increase was observed. In both cases no great difference in trajectory was found.

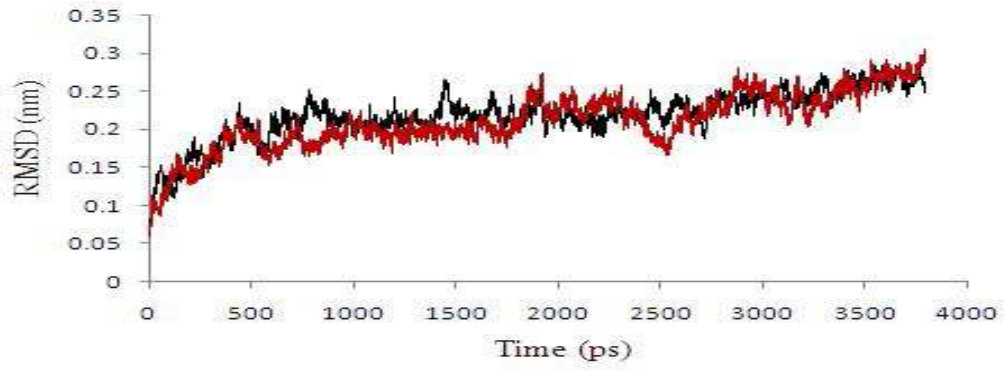

Fig. 4.39. Plot of root mean square deviation (RMSD) of backbone of VEGFR-2 unbound (red) and VEGFR-2-taxifolin complex (black) (Verma et al., Journal of Applied Pharmaceutical Science, 2012).

This analysis indicates that taxifolin showed remarkable stability for ATP-binding pocket and potentially competes with ATP. Number of H-bonds (cut off 0.35 nm)

which were formed during MD simulation between taxifolin and VEGFR-2 was also calculated. A variable profile was observed which fluctuate between 0 to 5 with an average value of 1.12 (Fig 4.40).

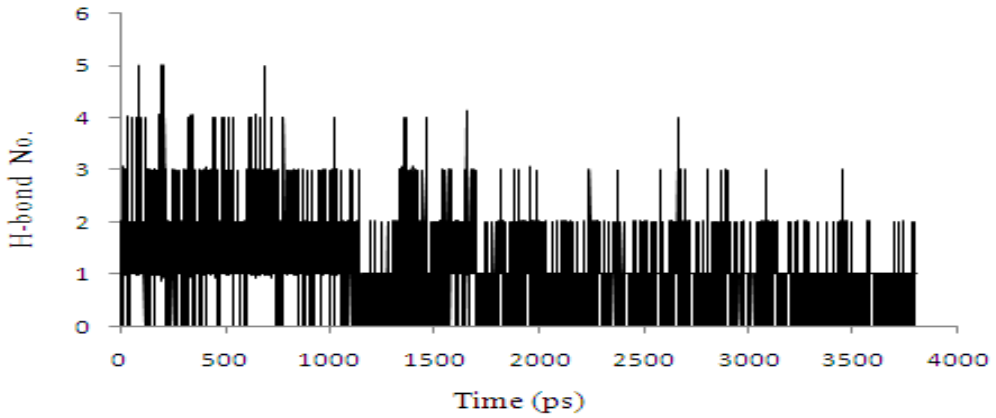

Fig. 4.40. Number of H-bonds formed during 3800 ps MD simulation (Verma et al., Journal of Applied Pharmaceutical Science, 2012).

Further to investigate the thermodynamic stability of complex during simulation, total energy and potential energy fluctuation were analyzed. All of these calculated properties of VEGFR-2 kinase-taxifolin complex showed very stable profile throughout the MD simulation.

Fig. 4.41 indicates that only few atoms of complex show higher fluctuation as compared to the unbound VEGFR-2.

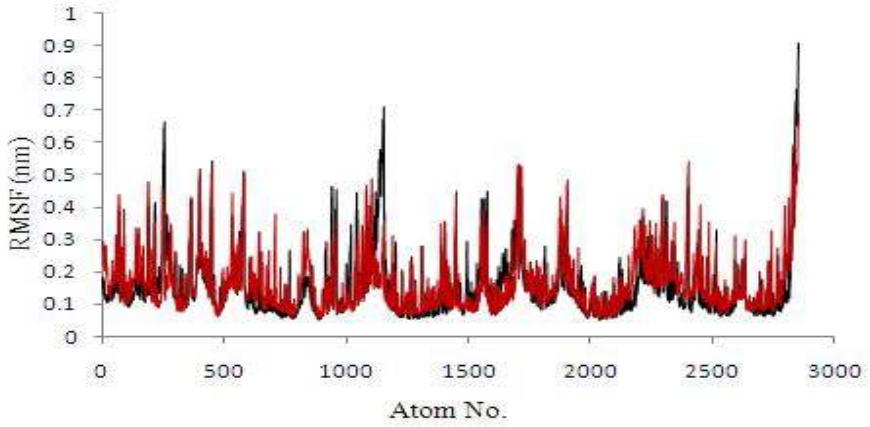

Fig. 4.41. Root mean square fluctuation (RMSF) of VEGFR-2 unbound (red) and VEGFR-2 kinase-taxifolin (black) atoms during 3800 ps MD simulation (Verma et al., Journal of Applied Pharmaceutical Science, 2012).

Additionally, RMSF of ATP-binding pocket residues was also analyzed to find out motion after binding with taxifolin (Fig 4.42).

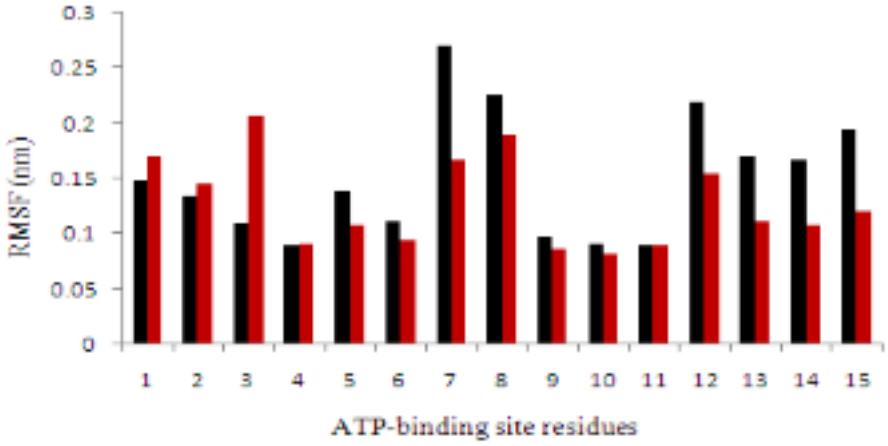

Fig. 4.42. Root mean square fluctuation (RMSF) of ATP-binding pocket residues (1-15: Leu 868, Glu 883, Lys 885, Glu 915, Phe 916, Cys 917, Lys 918, Phe 919, Gly 920, Asn 921, Leu 926, Arg 927, Ser 1035, Asp 1044 and Lys 1053) of VEGFR-2 unbound (red) and VEGFR-2 kinase-taxifolin (black) during MD simulation (Verma et al., Journal of Applied Pharmaceutical Science, 2012).

Earlier, there are mainly two types of inhibitor described for VEGFR-2: Type I inhibitors and Type II inhibitors. Type I inhibitors bind to the ATP binding site

through the formation of hydrogen bonds to the 'hinge' region residues (link between N and C-terminal lobes) and through hydrophobic interactions in and around the region as occupied by the adenine ring of ATP. These hydrogen bonds are similar to those normally formed by the exocyclic amino group of adenine. Type I inhibitors do not additionally require the DFG motif in the activation loop to adopt a 'DFG-out' conformation for binding (Traxler et al., 1999; Liu et al., 2006). Type II inhibitors typically use the ATP binding site along with hydrogen bonding and hydrophobic interactions made possible by residues of the activation loop being folded away from the conformation required for ATP phosphate transfer. Type II kinase inhibitors occupy a hydrophobic site that is adjacent to the ATP binding pocket created by a unique conformation of the activation loop (DFG-out) in which the phenylalanine residue of the DFG motif moves from its position in the kinase active conformation. Although occupying the allosteric site is characteristic of type II inhibitors, they can also extend into the adenine region and form one or two hydrogen bonds with kinase hinge residues in a manner similar to that of type I inhibitors (Liu et al., 2006). Analysis of molecular docking results and MD simulation poses at different time interval revealed that taxifolin is possibly acting as the Type I inhibitor. As described earlier taxifolin form H-bonds with hinge region residues: Leu 838, Glu 883, Glu 915 and Cys 917 (Fig. 2) and, additionally, found to form H-bond with activation loop residue Lys 1053 at different time interval of MD simulation. These interactions might lead to stable VEGFR-2 kinase (DFG-out conformation)-taxifolin complex during MD simulation (Fig. 4.43).

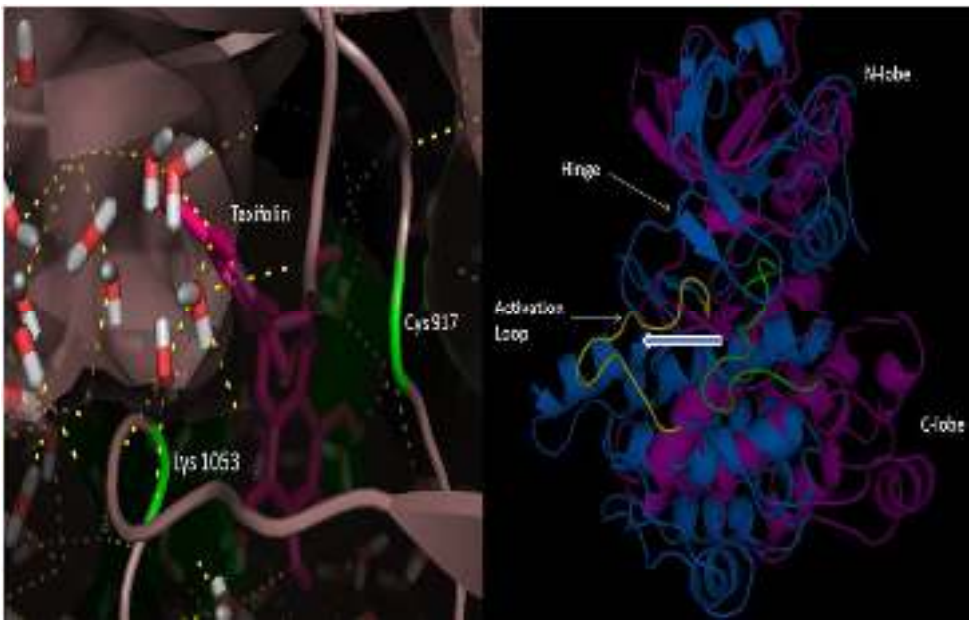

Fig. 4.43. Snapshot of system (VEGFR-2, taxifolin, water and counterions) at 3800 ps and conformational changes occurs in VEGFR-2 kinase during MD simulation (purple-0 ps, blue- 3800 ps, green-position of activation loop at 0 ps and yellow-position of activation loop at 3800 ps) (Verma et al., Journal of Applied Pharmaceutical Science, 2012).

4.2 In-vitro studies

4.2.1 Effect of quercetin and taxifolin on cell viability

Incubation of cells for 24 h with quercetin (20–500 μM) significantly decreased cell survival in a dose-dependent manner. Reduction in cell viability by ~50% in comparison with the control was achieved at a dose of 90 μM (Fig 4.44).

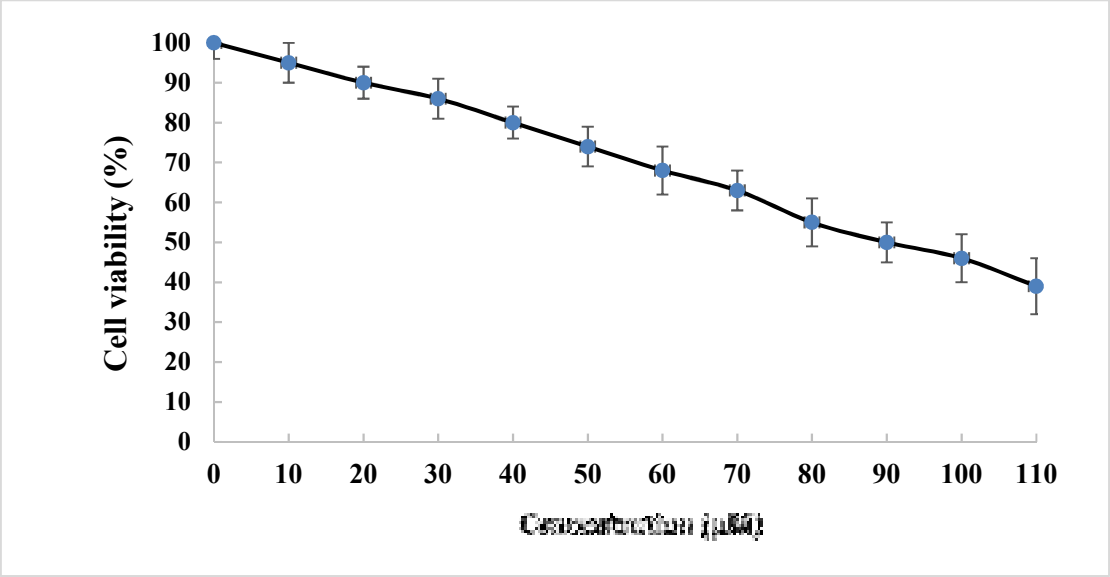

Fig. 4.44. Effect of quercetin on viability of HeLa cells. Data are represented as mean±SD of three determinations each performed in triplicate.

In contrast to quercetin treated cells, cells treated with DMSO showed little or no cytotoxicity. While in case of taxifolin (20–500 µM) ~50% reduction in cell viability was achieved at a dose of 400 µM (Fig 4.45).

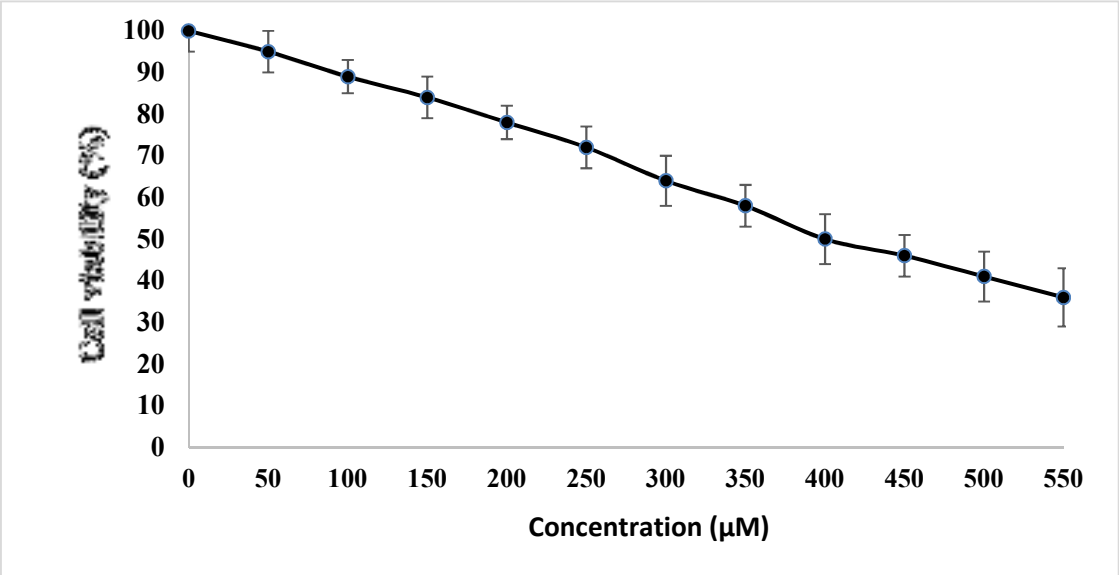

Fig. 4.45. Effect of taxifolin on viability of HeLa cells. Data are represented as mean±SD of three determinations each performed in triplicate.

4.2.2 DNA fragmentation assay

DNA ladder was in agarose gel electrophoresis in cells treated with quercetin (80 μM) and taxifolin (400 μM) incubated for 12, 24, 36 and 48 h (Fig. 4.46).

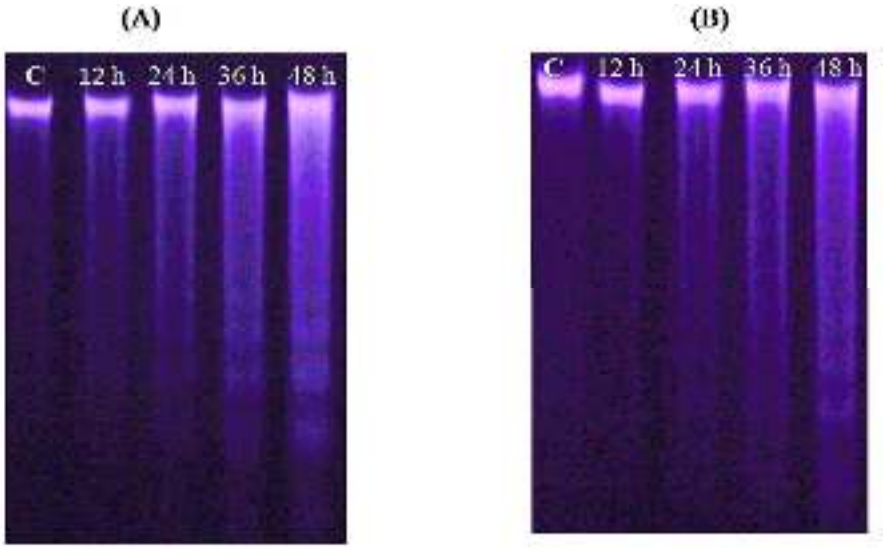

Fig. 4.46. (A) Quercetin-induced DNA fragmentation in HeLa cells, (B) taxifolin-induced DNA fragmentation in HeLa cells.

4.2.3 Effect of quercetin on markers of intrinsic apoptosis

Analysis of Bcl-2 family members (Bcl-2 and Bax), cytochrome c (cytosolic) and caspases -9 by RT-PCR analyses revealed a significant increase in the expression of Bax, cytochrome c and caspase -9 with decrease in the expression of Bcl-2 and in cells treated with quercetin and taxifolin compared to untreated control (Fig. 4.47, 4.48).

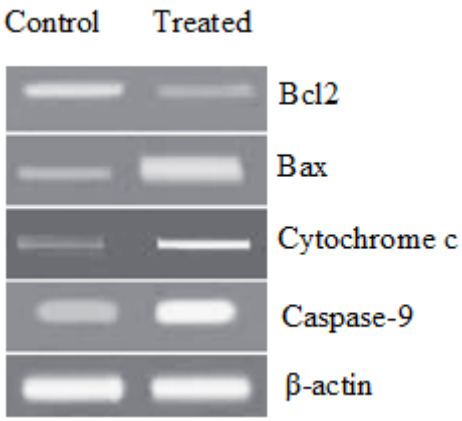

Fig. 4.47. Effect of quercetin on markers of intrinsic apoptosis in HeLa cells by RT-PCR analyses.

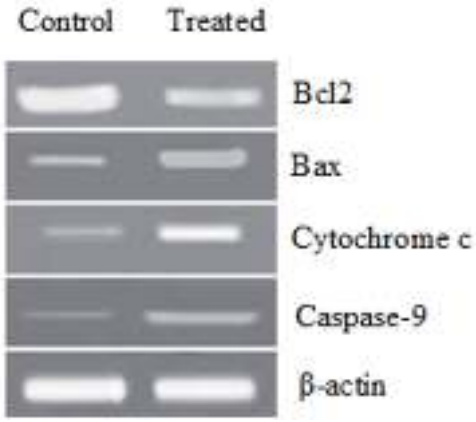

Fig. 4.48. Effect of taxifolin on markers of intrinsic apoptosis in HeLa cells by RT-PCR analyses.